

The *HST* Key Project on the Extragalactic Distance Scale XXVI.

The Calibration of Population II Secondary Distance Indicators and the Value of the Hubble Constant

Accepted for publication in the *Astrophysical Journal*

Laura Ferrarese^{1,2}, Jeremy R. Mould³, Robert C. Kennicutt, Jr.⁴, John Huchra⁵, Holland C. Ford⁶, Wendy L. Freedman⁷, Peter B. Stetson⁸, Barry F. Madore⁹, Shoko Sakai¹⁰, Brad K. Gibson¹¹, John A. Graham¹², Shaun M. Hughes¹³, Garth D. Illingworth¹⁴, Daniel D. Kelson¹², Lucas Macri⁵, Kim Sebo³, & N.A. Silberman⁹

ABSTRACT

A Cepheid-based calibration is derived for four distance indicators that utilize stars in the old stellar populations: the tip of the red giant branch (TRGB), the planetary nebula luminosity function (PNLF), the globular cluster luminosity function (GCLF) and the surface brightness fluctuation method (SBF). The calibration is largely based on the Cepheid distances to 18 spiral galaxies within $cz = 1500 \text{ km s}^{-1}$ obtained as part of the *HST* Key Project on the Extragalactic Distance Scale, but relies also on Cepheid distances from separate *HST* and ground-based efforts. The newly derived calibration of the SBF method is applied to obtain distances to four Abell clusters in

¹Hubble Fellow

²California Institute of Technology, Pasadena CA 91125, USA

³Research School of Astronomy & Astrophysics, Institute of Advanced Studies, ANU, ACT 2611, Australia

⁴Steward Observatory, The University of Arizona, Tucson AZ 85721, USA

⁵Harvard Smithsonian Center for Astrophysics, Cambridge MA 02138 USA

⁶Johns Hopkins University and Space Telescope Science Institute, Baltimore MD 21218, USA

⁷Carnegie Observatories, Pasadena CA 91101, USA

⁸Dominion Astrophysical Observatory, Victoria, British Columbia V8X 4M6, Canada

⁹NASA/IPAC Extragalactic Database and California Institute of Technology, Pasadena CA 91125, USA

¹⁰Kitt Peak National Observatory, NOAO, Tucson AZ 85726, USA

¹¹CASA, University of Colorado, Boulder, CO, USA

¹²Department of Terrestrial Magnetism, Carnegie Institution of Washington, Washington DC 20015, USA

¹³Royal Greenwich Observatory, Cambridge CB3 0HA, UK

¹⁴Lick Observatory, University of California, Santa Cruz CA 95064 USA

the velocity range between 3800 and 5000 km s⁻¹, observed by Lauer et al. (1998) using the *HST*/WFPC2. Combined with cluster velocities corrected for a cosmological flow model, these distances imply a value of the Hubble constant of

$$H_0 = 69 \pm 4(\text{random}) \pm 6(\text{systematic}) \text{ km s}^{-1} \text{ Mpc}^{-1}.$$

This result assumes that the Cepheid PL relation is independent of the metallicity of the variable stars; adopting a metallicity correction as in Kennicutt et al. (1998), would produce a $(5 \pm 3)\%$ decrease in H_0 . Finally, the newly derived calibration allows us to investigate systematics in the Cepheid, PNLf, SBF, GCLF and TRGB distance scales.

1. Introduction

Peculiar and infall velocities in the Local Supercluster are comparable to the Hubble flow. Consequently, H_0 cannot be determined by simply measuring the distances to a random assortment of nearby galaxies at velocities of a few hundred km s⁻¹. In view of this, the H_0 Key Project (Kennicutt, Freedman & Mould 1995, Freedman et al. 1998) was designed with three primary goals in mind: 1) to use a high quality primary standard candle, Cepheid variable stars, in nearby galaxies to calibrate reliable secondary distance indicators that are luminous enough to reach galaxies with heliocentric velocities up to ~ 10000 km s⁻¹, well beyond any substantial Hubble flow deviations. 2) To provide a check on potential systematic errors both in the Cepheid distance scale and the secondary methods. The Cepheid distance database from the *HST* Key Project can be used both to calibrate well-studied secondary methods, as well as to test the accuracy of other suggested indicators, and ultimately to calibrate them if they are found to be reliable. 3) To make direct Cepheid measurements of distances to three spiral galaxies in each of the Virgo and Fornax clusters.

Our primary goal of using the Cepheid period-luminosity (PL) relation to measure accurate distances to 18 carefully selected galaxies in the 3 – 20 Mpc range has been accomplished. We now turn our attention to the calibration of secondary distance indicators for extension into the smooth Hubble flow. The need for a multiplicity of calibrators goes beyond square-root-n considerations: much of the current uncertainty in the distance scale stems from the likelihood of systematic errors that are not fully understood, together with uncertainties in the dispersion of secondary distance indicators, which affects their use through Malmquist bias. Other papers in this series will calibrate the Tully-Fisher relation (Sakai et al. 1999), the D_n - σ relation and the fundamental plane (Kelson et al. 1999), and the Type Ia supernovae (Gibson et al. 1999). In this paper we use Cepheid distances to calibrate four additional distance indicators: the luminosity of the tip of the red giant branch (TRGB), the planetary nebula luminosity function (PNLF), surface brightness fluctuations (SBF), and the globular cluster luminosity function (GCLF). Because all of these secondary candles utilize stars in old stellar populations, we imprecisely refer to them as

Population II distance indicators, without implying that the stars are necessarily metal poor. The calibrations in subsequent sections will illustrate the relative strengths and weaknesses of the four Pop II distance indicators, and show where more work must be done on particular indicators.

Of the distance indicators discussed in this paper, at present only the SBF method has the potential of reaching the unperturbed Hubble flow. Thanks to the *HST* Near Infrared Camera and Multi Object Spectrometer (NICMOS) galaxies as far as $cz = 10000 \text{ km s}^{-1}$ are within sight (Jensen et al. 1999). SBF measurements currently point to values of H_0 around $80 \text{ km s}^{-1} \text{ Mpc}^{-1}$. In particular, velocities and distances to the four Abell clusters in the $3800\text{--}5000 \text{ km s}^{-1}$ velocity range observed with the *HST*/WFPC2 by Lauer et al. (1998), while leading directly to $H_0 = 82 \pm 8 \text{ km s}^{-1} \text{ Mpc}^{-1}$, also allowed the calibration of the far field brightest cluster galaxies Hubble diagram of Lauer and Postman (1992), giving $H_0 = 89 \pm 10 \text{ km s}^{-1} \text{ Mpc}^{-1}$. In a very recent preprint, Tonry et al. (1999) combined their latest calibration of the ground-based *I*-SBF method with a sophisticated model for large scale velocity flows to derive $H_0 = 77 \pm 8 \text{ km s}^{-1} \text{ Mpc}^{-1}$. Finally, Thomsen et al. (1997) derive $H_0 = 71 \pm 11 \text{ km s}^{-1} \text{ Mpc}^{-1}$ from the SBF distance to NGC 4881 in the Coma cluster.

The usefulness of TRGB, PNLf and GCLF methods resides mainly in providing cross checks as to the reliability of each indicator. In addition, all of the distance indicators presented in this paper have the indisputable merit of being applicable to both spiral and elliptical galaxies. As such they serve as a much needed link between the Cepheid distance scale and early type galaxies. This link cannot be provided by the Tully-Fisher relation, nor the $D_n - \sigma$ and the fundamental plane, which are exclusive to spirals and ellipticals respectively.

TRGB distance estimates are routinely performed in the Local Group, even if the use of *HST* has brought the Leo I group, and even Virgo into sight (Sakai et al. 1997, Ferguson et al. 1998, Harris et al. 1998). GCLF measurements beyond the Virgo and Fornax clusters are technically extremely challenging, as testified by the *HST* observations of the Coma galaxy IC 4051 (Baum et al. 1995, 1997). The wide range of H_0 values derived from GCLF measurements in the Virgo and Fornax clusters, ranging from the mid 50s (Sandage & Tammann 1996) to the low 80s $\text{km s}^{-1} \text{ Mpc}^{-1}$ (Grillmair et al. 1998), can be traced back to uncertainties in the peculiar and infall velocities for these clusters, and to the still rather uncertain calibration of the method itself. Finally, PNLf measurements become prohibitive for galaxies beyond $\sim 40 \text{ Mpc}$ even using 8-m class telescopes (Jacoby 1998). Distances to Virgo and Fornax suggest values of H_0 in the upper 70s to mid 80s $\text{km s}^{-1} \text{ Mpc}^{-1}$ (Jacoby, Ciardullo & Ford 1990, McMillan, Ciardullo & Jacoby 1993, Ford et al. 1996)

As a first step in calibrating the Pop II distance indicators presented in this paper, we compiled a database of all available Cepheid, TRGB, PNLf, GCLF and SBF measurements. The results are published separately in Ferrarese et al. (1999, hereafter F99). Here we will use the distance database not only to provide a Cepheid calibration for TRGB, PNLf, GCLF and SBF, but also to test each method, and the Cepheid distance scale itself, for biases. This paper

is organized as follows. A brief overview of the Cepheid calibration adopted and the steps taken to prepare the database for the derivation of the magnitude zero points, are discussed in §2. The distance indicators are then considered, from the least to the most far reaching ones: TRGB, PNLF, GCLF and SBF are calibrated in §3 though §6, and the results discussed in §7. There we will compare the different methods and discuss the magnitude of the metallicity dependence of the Cepheid PL relation, and its effects on the calibrations derived in the previous sections. The newly calibrated SBF distances to clusters beyond $cz = 3800 \text{ km s}^{-1}$ are discussed in §8, and a value for the Hubble constant is derived. A summary of conclusions can be found in §9.

2. Cepheid Distances and Preparation of the Database

A compilation of all Cepheid distances obtained as part of the H_0 Key Project, as well as independent ground-based and *HST* efforts is given in F99. In that paper, all distances are placed on a homogeneous system, with consistent calibration and fitting of the PL relation, treatment of the extinction corrections, and estimate of the errors. Here we will only remind the reader that the PL relation is calibrated on a sample of 32 LMC Cepheids with *BVI* photoelectric photometry and periods in the range $1.6 < P < 63$ days (Madore & Freedman 1991), and assumes a true distance modulus and average line-of-sight reddening to the LMC of 18.50 ± 0.13 and $E(B - V) = 0.10$ mag respectively, a ratio of total to selective absorption $R_V = A(V)/E(B - V) = 3.3$, and a reddening law following Cardelli, Clayton and Mathis (1989). The derived distances do not appreciably depend on variations in R_V , or on the adopted $E(B - V)$ and reddening law for the LMC (Ferrarese et al. 1996, F99)

Those galaxies having distances that had to be modified to adhere to the criteria listed above (SMC, NGC 3109, NGC 1365, NGC1425, NGC 1326A, NGC 4535) and galaxies with distances that will not be considered for calibrating secondary distance indicators (NGC 2403, GR8, NGC 2366, and NGC 4571) are discussed in detail in F99.

Because no consensus has yet been reached on the issue of a dependence of the Cepheid PL relation on the metallicity of the variable stars (e.g. see Kennicutt et al. 1998), we prefer not to include metallicity effects explicitly in the Cepheid distances listed in the F99 database, but we will discuss the impact of a metallicity dependence on the distances and the calibration of secondary distance indicators in §7.2.

In the F99 database, distance moduli are given only for the Cepheid measurements. For the other indicators, magnitudes (the magnitude of the tip of the RGB, the cutoff magnitude of the PNLF, the turnover magnitude of the GCLF and the fluctuation magnitude for SBF), rather than distances, are given. To provide a consistent dataset, these magnitudes are not corrected for reddening. Unlike the Cepheids (e.g. Freedman et al. 1994) the secondary distance indicators can only be corrected for the effects of foreground extinction, as no estimate of the internal reddening is available. This is not as big a handicap as it might appear as regions suitable

for SBF measurements, PNe, TRGB stars and globular clusters are all found in areas relatively free of internal dust absorption (Tonry & Schneider 1988, Feldmeier, Ciardullo & Jacoby 1997, Whitmore 1996). Estimates of the foreground reddening $E(B - V)$ are available from the HI maps of Burstein and Heiles (1984), or from the 100 μm maps reprocessed from IRAS/ISSA and COBE/DIRBE data by Schlegel et al. (1998). The two methods show a systematic difference in the values of $E(B - V)$ of about 0.02 mag (the DIRBE/IRAS maps giving higher reddenings), the cause of which is not yet understood. In this paper, the DIRBE/IRAS maps have been adopted: they have higher angular resolution, provide a more direct measure of the dust column density, and are more accurate than the HI maps, especially in regions of moderate and high reddenings. For comparison, magnitude zero points derived using Burstein & Heiles reddenings will also be presented in the Appendix. As a word of caution, we need to point out that recent findings claim that reddenings from DIRBE/IRAS maps might be overestimated by up to 50% in regions of high extinction [$E(B - V) > 0.15$ mag] (Arce & Goodman 1999). Because the Galactic reddening for all of our galaxies is smaller than $E(B - V) \sim 0.1$ mag, these findings do not directly concern our analysis. The reddening law used to convert $E(B - V)$ values to extinction in different passbands is from Cardelli, Clayton and Mathis (1989). The value of R_V for the diffuse interstellar medium is $R_V = 3.1$, which is generally derived from early type stars (Schultz & Wiemer 1975, Whittet & van Breda 1980, Rieke & Lebofsky 1985). To account for the convolution of the broad band filters and the redder spectral energy distribution of the Pop II objects considered in this paper (globular cluster, elliptical galaxies) a value of $R_V = 3.3$ has been adopted for all distance indicators with the exception of PNLf. PNe are observed in a narrow band filter, therefore $R_V = 3.1$ is the appropriate value to use¹⁵. Note that all of the distance indicators considered in this paper are little affected by internal extinction (the contribution of which is neglected), therefore the low internal R_V claimed for elliptical galaxies ($\sim 2.1 - 3.3$, Goudfrooij et al. 1994) is not an issue. A treatment of errors associated with the extinction corrections is given in Appendix A.

3. Calibration of the Tip of the Red Giant Branch Method

Reviews of the tip of the red giant branch (TRGB) method as a distance indicator are given by Madore, Freedman & Sakai (1996) and Sakai (1999). Briefly, the TRGB marks the He ignition in the degenerate core of low mass stars. The core mass is constant for stellar ages larger than a few Gyrs, thereby producing a constant luminosity for the Helium flash. The absolute I magnitude of the TRGB proves to be fairly invariant over a wide range of metallicity (Da Costa & Armandroff 1990, Lee, Freedman & Madore 1993, Salaris & Cassisi 1998), making the TRGB a powerful standard candle.

Unlike the PNLf, GCLF and SBF methods, TRGB is not currently calibrated using

¹⁵For $R_V = 3.3$, the extinction curves of Cardelli et al. give the following ratios for the absorption: $A(B) : A(5007) : A(V) : A(I) : A(F814W) : A(K_s) : A(K') = 1.288:1.120:1:0.600:0.596:0.120:0.125$.

Cepheids. Two calibration philosophies are being pursued, leading to a 0.15 mag discrepancy in the absolute I magnitude of the tip (Lee, Freedman & Madore 1993, Salaris & Cassisi 1998). In the range of metallicities $-2.35 < [\text{M}/\text{H}] < -0.28$ dex [corresponding to $1.2 < (V - I)_{-3.5} < 2.2$ mag, where $(V - I)_{-3.5}$ is the color measured at an absolute I magnitude of -3.5], the Salaris and Cassisi calibration produces a quadratic dependence of M_I^{TRGB} on metallicity, with $-4.25 \leq M_I^{\text{TRGB}} \leq -4.15$ mag. In contrast, Lee et al. find that M_I^{TRGB} varies between -3.9 and -4.1 mag for $-2.17 < [\text{Fe}/\text{H}] < -0.71$ [$1.2 < (V - I)_{-3.5} < 1.8$ mag]. The discrepancy is due entirely to different estimates of the TRGB bolometric luminosity, which Salaris & Cassisi adopt from theoretical stellar models (Salaris & Cassisi 1996), while Lee et al. adopt from the empirical observations of Galactic globular clusters with RR-Lyrae distances (Da Costa & Armandroff 1990, Frogel, Persson & Cohen 1983). The latter calibration elevates the TRGB to the rank of primary distance indicator, similar to the Cepheids.

In this paper, we will treat the TRGB as a secondary distance indicator, and provide a calibration through the Cepheids. This will allow us to perform a consistency check between the primary TRGB calibration and the Cepheid distance scale. Furthermore, the relative insensitivity of the TRGB to metallicity, and the lack of correlation between the halo and Cepheid metallicity, provides an independent way to test the metallicity dependence of the Cepheid PL relation (Lee et al. 1993, Kennicutt et al. 1998), this will be discussed in §7.2. For present purposes, we do not apply any metallicity correction to the TRGB magnitudes. Over the range of metallicities spanned by the TRGB calibrators [$1.1 < (V - I)_{-3.5} < 1.6$ mag], the Lee et al. and Salaris & Cassisi estimates disagree not only on the magnitude of such correction (which are however small, within 0.1 mag), but also on their sign.

From F99, all galaxies with both Cepheid distances and an estimate of the TRGB I magnitude belong to the Local Group: LMC, Sextans A and B, IC 10, IC 1613, M31, M33, NGC 3109 and NGC 6822. For these galaxies, a Cepheid – TRGB comparison is shown in Figure 1 (assuming no metallicity dependence of the Cepheid PL relation or the TRGB magnitudes), and leads to a magnitude zero point

$$M_I^{\text{TRGB}} = -4.06 \pm 0.07 \text{ (random)} \pm 0.13 \text{ (systematic)} \text{ mag.} \quad (1)$$

We must stress that the large errors in the $(V - I)$ colors prevent us from quantifying a color (metallicity) dependence of M_I^{TRGB} , and therefore equation (1) applies correctly only at the sample mean $(V - I) \sim 1.42$ mag. The fit leading to equation (1) is done accounting for errors in both Cepheid distances and TRGB magnitudes; the random error is the 1σ error in the fit, while the systematic error is the combination, in quadrature, of the uncertainty in the LMC distance (0.13 mag) and the uncertainty in the zero point of the LMC PL relation (0.02 mag, see §8). Adding to the above calibrators the (almost) direct comparison between the Cepheid distance to M81 and the M_I^{TRGB} for the M81 dwarfs BK5N and F8DI, produces the minor adjustment $M_I^{\text{TRGB}} = -4.05 \pm 0.06$ mag (random error only). A calibration of M_I^{TRGB} based on group

distances is not as robust as the calibration given in equation (1), because TRGB observations outside the Local Group and the M81 group are available to only one galaxy in each of the Leo I group, the M87 subcluster in the Virgo cluster (see F99 for a discussion of the spatial subdivision of the Virgo cluster into separate subclusters) and the NGC 5128 group, and therefore cluster depth effects are likely to affect the group distances. Using group distances to the four groups mentioned above, not weighted by their spatial extent, would lead to $M_I^{TRGB} = -4.00 \pm 0.05$ mag, in good agreement with the result given in equation (1). The magnitude zero points discussed in this section and in §4–6 are listed in Table 1. In that table, the reduced χ^2 of the fit can be found in parentheses next to each zero point; the underline identifies the magnitude zero points which we consider most trustworthy for each indicator.

Figure 2 shows a comparison between the secondary calibration presented in equation (1) and the primary calibration of the TRGB. The top panel shows the color dependence of the absolute I magnitude of the TRGB predicted by Lee et al. (dashed line) and Salaris and Cassisi (the solid and dotted lines differ exclusively for the adopted bolometric correction, the dotted line is based on the stellar models of Kurucz 1979, the solid line on the Yale isochrones). The lower panel shows the Cepheid – TRGB distance moduli residuals when the calibration given in equation (1) is applied (solid dots and error bars). It is quite obvious that the large uncertainty in distance moduli (and in colors, which are not plotted in the figure) prevent testing the correlation between the residuals and the colors. The Lee et al. calibration would lead to the residuals shown by the open circles, with a mean shown by the dashed line, while the Salaris & Cassisi calibration (simply for illustration we chose the Kurucz models) produces the residuals shown by the stars, with a mean given by the dotted line. The Cepheid calibration is virtually indistinguishable from the Lee et al. (1993) primary calibration, and agrees with the Salaris & Cassisi (1998) calibration at the 1.2σ level (we assume a 0.1 mag uncertainty for the primary calibrations). Therefore, Salaris & Cassisi’s claim that the 0.1–0.2 mag level disagreement between their TRGB calibration and the Cepheid distance scale is statistically significant seems premature at this point, in view of the large uncertainties. Furthermore, the perfect agreement between the Lee et al. calibration (which bypasses the Cepheids completely, relying only on RR-Lyrae distances to Galactic globular clusters) and the Cepheid calibration (based on an assumed distance to the LMC), is a strong reassurance as to the reliability of our adopted LMC distance and error.

4. Calibration of the Planetary Nebula Luminosity Function Method

Reviews of the Planetary Nebula luminosity function (PNLF) and its application as a distance indicator are given by Jacoby et al. (1992), Jacoby (1996), Mendez (1998) and Jacoby, Ciardullo & Feldmeier (1998). PNe owe their role of standard candles to the universality of their luminosity function. Because PNe are high excitation objects, the LF is measured at the $[\text{OIII}]\lambda 5007$ emission line, and it is approximated by a semiempirical formula which combines theoretical models with the sharp cutoff at the bright end (characterized by a ‘cutoff’ magnitude m^*) observed for the

PNLF in the bulge of M31 (Ciardullo et al. 1989). Effects of metallicity, population age, Hubble type and absolute luminosity of the parent galaxy are claimed to be negligible (Jacoby & Ciardullo 1999; Ciardullo & Jacoby 1992; Jacoby 1996; Dopita et al. 1992; Stanghellini 1995; Jacoby, Ciardullo, & Harris 1996; McMillan, Ciardullo & Jacoby 1993; Jacoby, Walker & Ciardullo 1990). Potential sources of biases are contamination by HII regions in spiral galaxies, by background emission line galaxies at $z = 3.1$ (Jacoby, Ciardullo & Harris 1996, Ciardullo et al. 1998), and by intracluster PNe (Ciardullo et al. 1998). HII regions should not present a serious threat since they can be discriminated from PNe based on their $H\alpha/[OIII]$ ratio; however intracluster PNe can lead to an underestimate of the PNLF cutoff magnitude (and therefore the PNLF distance) by up to 0.2 mag in rich clusters (Mendez 1998). PNLF measurements are performed routinely in both spiral and elliptical galaxies reaching as far as the Virgo and Fornax cluster (Jacoby, Ciardullo & Ford 1990, McMillan, Ciardullo & Jacoby 1993, Ciardullo et al. 1998), but unfortunately exposure times become prohibitive for galaxies beyond ~ 40 Mpc even using 8-m class telescopes (Jacoby et al. 1998).

The absolute magnitude corresponding to m^* is currently calibrated solely by the Cepheid distance to M31 from Madore & Freedman (1991), giving $M^* = -4.54$ mag (at $\lambda = 5007$ Å, e.g. Ciardullo et al. 1998). However, the PNLF has now been measured in six galaxies with Cepheid distances (F99). These are the LMC, M31, M81, M101, NGC 300 and NGC 3368 in the Leo I group. A comparison of Cepheid distance moduli and PNLF cutoff magnitudes m^* for these galaxies is shown in Figure 3, and produces an absolute cutoff magnitude

$$M^* = -4.58 \pm 0.07 \text{ (random)} \pm 0.13 \text{ (systematic) mag,} \quad (2)$$

assuming no metallicity dependence of the Cepheid PL relation. As for all other secondary distance indicators presented in this paper, the fit is performed accounting for errors in both coordinates. Because the calibration of PNLF is based on both ground-based and *HST* Cepheid galaxies (unlike TRGB, which is based exclusively on ground-based galaxies, and GCLF and SBF which are based exclusively on *HST* galaxies), a 0.09 mag error has been added in quadrature to the distance moduli for the *HST* galaxies prior to performing the fit. This term accounts for the (in this case) random error associated with the *HST* photometry, and is not included explicitly in the error on the distance moduli quoted in F99. The calibration in equation (2), which we consider the most robust to date, reproduces the M31-based calibration of Ciardullo & Jacoby within 0.04 mag, in spite of the different Galactic reddenings adopted. There are five groups/clusters with both PNLF and Cepheid mean distances. These are the NGC 1023 group, the Leo I group, the M87 and NGC 4472 subclusters, and the Fornax cluster; the NGC 4649 subcluster in the Virgo cluster has been excluded as it deviates by more than 3σ from the best fit. The indirect comparison of PNLF magnitudes and Cepheid distances to these groups (excluding the Leo I groups for which there is a direct comparison) can be added to the direct calibrators. To provide meaningful weighting, a measure of the group/cluster depth (based on the projected extent of the group in the sky as listed in Table 2), is added to the uncertainty in the group mean

Cepheid distances. This leads to a zero point of $M^* = -4.61 \pm 0.06$ mag, consistent with the above adopted calibration.

5. Calibration of the Globular Cluster Luminosity Function Method

Reviews of the GCLF method can be found in Harris (1991), Harris (1996) and Whitmore (1996). The use of globular cluster systems for distance determinations relies on the empirical result that their luminosity function is remarkably well approximated by a Gaussian (e.g. Abraham & van den Bergh 1995) with the turnover M_T acting as a standard candle. The calibration of M_T is still rather controversial (Secker 1992, Sandage & Tammann 1995, Whitmore et al. 1996, Della Valle et al. 1998); furthermore, reliable estimates of the GCLF turnover magnitudes require deep photometry that sample the GCLF well over the turnover. The latter requirement is due to the fact that the dispersion of the GCLF is not universal, but rather shows a large scatter both within late type spirals (e.g. in the V band $\sigma = 1.10$ mag for M31 while $\sigma = 1.42$ mag for the Milky Way, Secker 1992, see also the result obtained by Bothun et al. 1992 on NGC 7814), and early type galaxies (e.g. $\sigma = 1.67$ mag for the E0 NGC 5481, Madejsky & Rabolli 1995, while $\sigma = 1.09$ mag for the E1 NGC 4494, Forbes 1996).

The existence of second parameters affecting M_T has been widely discussed in the literature. There are claims that M_T depends on the luminosity of the parent galaxy, brightening by about 0.3 V magnitudes going from dwarf systems to giant ellipticals (Whitmore 1996); on the environment, being fainter for galaxies in rich clusters (Blakeslee & Tonry 1996); and on Hubble type, being ~ 0.15 V mag brighter in spirals than ellipticals (Whitmore 1996). This last observation has been attributed by Ashman, Conti & Zepf (1995) to metallicity variations. There is evidence that the luminosity function of the metal poor and metal rich clusters do not peak at the same magnitude in the sense of the blue clusters being brighter (Elson & Santiago 1996, Kundu et al. 1999, Kundu and Whitmore 1998). Finally, contamination by a spatially extended GC component associated with tidal debris, and not necessarily linked to any particular galaxy (much as is the case for intracluster PNe, see §4), should be taken into account (West et al. 1995).

Traditionally, GCLF measurements have been performed preferentially in the Johnson B or V bands. The lack of color information, and the (not well defined) dependence of globular cluster color on the luminosity of the host galaxy calls for an independent calibration of the GCLF in these two bands. The most up-to-date calibration of the V band GCLF is by Whitmore et al. (1996). Based on the weighted means of the turnover magnitudes for six Virgo ellipticals and the Cepheid distances to NGC 4321, NGC 4496A and NGC 4536, the absolute V magnitude of the GCLF turnover is found to be $M_V^T = -7.21 \pm 0.26$ mag. This calibration is in agreement with the one derived by Secker (1992) based on RR Lyrae distances for the Milky Way globular clusters, $M_V^T = -7.29 \pm 0.13$ mag (but see also Sandage & Tammann 1995); however, Secker (1992) also notes that a calibration based solely on the distance to M31 (to date the only galaxy with both a GCLF and Cepheid distance) would lead to the discrepant value $M_V^T = -7.69 \pm 0.15$ mag (Secker's

result was modified here to adopt the M31 Cepheid distance from Madore and Freedman 1991.)

The Whitmore et al. calibration can now be improved using the F99 database, which includes a more homogeneous and reliable set of GCLF measurements (many GCLF turnover magnitudes used by Whitmore are derived from data that do not properly sample the turnover, and a few are based on B , rather than V –band measurements) and a larger sample of Cepheid distances.

An indirect calibration of the V –band GCLF can be derived using group distances to the M87 subcluster, the NGC 4472 subcluster, and the Fornax cluster. The GCLF turnover magnitude is defined by M87 and NGC 4478 for the M87 subcluster, and by NGC 4472 for the NGC 4472 subcluster. The turnover magnitudes are within 0.03 mag, as expected if the two subclusters are at approximately the same distance as supported by the PNLf and SBF observations presented in this paper (see also Gavazzi et al. 1999). Since M87 is at the bottom of the potential well of the cluster (Böhringer et al. 1994), M87 and NGC 4472 should give a good estimate of the cluster mean distance. The mean turnover magnitude of the Virgo cluster is 23.68 ± 0.06 mag in V , 0.2 mag brighter than estimated by Whitmore (1996). The Cepheid distance modulus to Virgo, defined by NGC 4321, NGC 4496A, NGC 4536, NGC 4548 and NGC 4535 is 31.03 ± 0.03 mag, or 0.07 mag fainter than the value adopted by Whitmore. The resulting V turnover magnitude for Virgo is -7.35 ± 0.07 mag. Since Whitmore’s calibration, Cepheid and GCLF distances have become available for the Fornax cluster. The GCLF mean turnover magnitude to Fornax is defined by NGC 1344, NGC 1380, NGC 1399 and NGC 1404, while the mean Cepheid distance is defined by NGC 1326A, NGC 1425 and NGC 1365. This gives a turnover magnitude of -7.85 ± 0.07 , *a full 0.5 magnitudes brighter than that found for the Virgo cluster*. Of the four GCLF galaxies in Fornax, NGC 1344, NGC 1399 and NGC 1380 are found within 0.06 mag of each other, while NGC 1404 is 0.28 ± 0.14 mag in the background, but still consistent with it belonging to the cluster, for which we estimate a depth of ~ 0.3 mag from the projected extent of the cluster in the sky. A formal weighted mean of the Virgo and Fornax absolute magnitudes of the turnover, for no metallicity correction of the Cepheid PL relation, gives (Figure 4):

$$M_V^T = -7.60 \pm 0.25 \text{ (random)} \pm 0.16 \text{ (systematic) mag.} \quad (3)$$

The random error quoted in the equation above reflects the actual scatter seen in the data, rather than the formal uncertainty in the fit. The observed scatter is incompatible with the published internal errors in the GCLF measurements, and the expected uncertainty due to cluster depth effects, pointing to the existence of second parameters. The systematic error is a combination of the uncertainty in the PL calibration, the error in the distance to the LMC and the error affecting the *HST* photometry (see §8). The latter are of a systematic rather than random nature, because all Cepheid galaxies used for the calibration of GCLF were observed with the same *HST* instrumental configuration. The magnitude zero point in equation (3) is consistent with the result obtained using a comparison of Cepheid and GCLF distances for M31, $M_V^T = -7.70 \pm 0.19$ mag, however the discrepancy between the M_V^T values for Virgo and Fornax is worrisome, and

is evident in the large reduced χ^2 of the fit (~ 12 , from Table 1). It is difficult to imagine a scenario in which such a large discrepancy could be due to a different spatial distribution of the Cepheid and GCLF galaxies within the two clusters. The sense of the discrepancy is such that the Cepheid galaxies would be foreground to the Virgo cluster, and background to the Fornax cluster, assuming the centers of the clusters to be defined by the GCLF galaxies; however, both PNLF and SBF sample the central ellipticals in Virgo and Fornax, and give a consistent Virgo-Fornax relative distance of ~ 0.35 mag, with Fornax being further, while GCLF places Fornax and Virgo at practically the same distance. Based on the current evidence, we conclude that at present, the GCLF method carries an unexplained uncertainty that may be quite large. The limited amount of data makes it difficult to establish whether this is due to the fact that the GCLF itself is not a standard candle, or to problems in the published GCLF measurements, for example arising from incorrect estimates of the incompleteness of the data or contamination by background galaxies.

The situation for the B -band GCLF is more precarious still, as the sample of available measurements is very limited. The only direct calibration available in the literature for the B -band GCLF was provided by Harris et al. (1991) based on 75 halo clusters with RR Lyrae distances, giving $M_B^T = -6.84 \pm 0.17$ mag. There are four groups for which a mean Cepheid distance and GCLF B turnover magnitude can be defined: the NGC 4472 and NGC 4639 subclusters in Virgo, the Fornax cluster and the Leo I group. A formal fit gives (Figure 4):

$$M_B^T = -7.02 \pm 0.5 \text{ (random)} \pm 0.16 \text{ (systematic) mag.} \quad (4)$$

As for the case of the calibration of M_V^T , the random error reflects the actual scatter seen in the data. As was the case for the V -band GCLF, the points show an uncomfortably large dispersion: M_B^T is -6.33 ± 0.23 mag, -6.98 ± 0.10 mag, and -7.48 ± 0.26 mag, for Virgo, Fornax and Leo I respectively. Excluding the NGC 4649 subcluster, for which we find in §4 and §6 a large Cepheid distance compared to both PNLF and SBF measurements, leads to $M_B^T = -6.95 \pm 0.5$ mag.

6. Calibration of the Surface Brightness Fluctuation Method

The surface brightness fluctuation (SBF) method was first introduced by Tonry & Schneider (1988); reviews can be found in Jacoby et al. (1992), Tonry et al. (1997) and Blakeslee, Ajhar & Tonry (1999). The method can be applied to both elliptical galaxies and the dust-free bulges of early-type spirals. The fluctuation magnitude, \overline{m} , measures the amplitude of the luminosity fluctuations arising from the counting statistics of the stars contributing to the flux in each pixel of a high S/N image. \overline{m} is heavily dominated by RGB stars, and therefore its absolute calibration \overline{M} is strongly wavelength and color (metallicity) dependent.

To date, the largest SBF survey is the ground-based effort by Tonry et al. (1999) in the

Kron-Cousins I -band, which comprises over 300 galaxies within $cz = 4000 \text{ km s}^{-1}$. With *HST*/WFPC2 and the F814W filter, data extending to the Coma cluster have been obtained (Thomsen et al. 1997). In the future, the emphasis of SBF is expected to shift to the near-infrared, where SBF magnitudes are brighter and dust contamination is less threatening (e.g. Blakeslee, Ajhar & Tonry 1999). A few galaxies have been observed in the K' ($\lambda_c = 2.10\mu\text{m}$) and K_s ($\lambda_c = 2.16\mu\text{m}$) bands (Jensen et al. 1998, Pahre & Mould 1994), and using *HST*/NICMOS (Jensen et al. 1999). Because of the small size of these IR surveys (the *HST*/NICMOS data have not been published at the time of writing this paper), we limit the present discussion to the I and F814W SBF, and touch briefly on the K' and K_s surveys in Appendix B. Five dwarf elliptical galaxies in the Sculptor group have been observed in the R -band by Jerjen, Freeman & Binggeli (1998). Because of the lack of overlap between this sample and any other Cepheid or SBF sample, the R -band SBF must be calibrated using stellar population synthesis models, and will not be discussed in this paper.

6.1. I -band SBF

A Cepheid-based calibration of the I -SBF method is given by Tonry et al. (1999) as $\overline{M}_I = (-1.74 \pm 0.07) + (4.5 \pm 0.25)[(V - I)_0 - 1.15] \text{ mag}$, where $(V - I)_0$ is the galaxy unreddened color determined in the same region where the fluctuations are measured. The zero point is derived by Tonry et al. using the median for six galaxies with SBF measurements and Cepheid distances (from F99). The slope of the \overline{M}_I vs $(V - I)_0$ relation was determined by Tonry et al. (1997) by simultaneously fitting all of the galaxies in groups and clusters for a single value of the slope and a different zero point for each group. The slope thus derived is in perfect agreement with the predictions of stellar population models (Worthey 1993, 1994), which also predict a zero point of -1.81 mag , in good agreement with Tonry et al. (1999).

For the purpose of this paper, we do not attempt to recalibrate the color dependence of the SBF magnitude, but rather adopt the 4.5 slope from Tonry et al. (1997). The galaxies with both Cepheid distances and I -SBF magnitudes are M31, M81, NGC 3368 in Leo I, NGC 4725 in the Coma II cloud, NGC 4548 in the Virgo cluster, and NGC 7331. A comparison for these galaxies is shown in Figure 5, where the fluctuation magnitudes are corrected for extinction (see §2), and for the color dependence. A weighted least-squares fit gives:

$$\overline{M}_I = [-1.79 \pm 0.09(\text{ random}) \pm 0.16(\text{ systematic})] + (4.5 \pm 0.25)[(V - I)_0 - 1.15] \text{ mag}. \quad (5)$$

The difference between the zero point above and the one derived by Tonry et al. (1999) is due to two factors. Tonry et al. use the extinction law from Schlegel et al. (1998) rather than adopting the same law used in deriving the Cepheids distances (from Cardelli Clayton & Mathis 1989). Second, Tonry et al. (1999) use a median of the zero points given by all calibrators rather

than a weighted mean. This effectively rejects NGC 7331 which not only produces the brightest zero point (Figure 5), but also carries a large weight in our weighted mean, having smaller error bars than the other galaxies. Choosing between the zero point presented in this paper and the one given by Tonry et al. (1999) is largely a matter of personal preference, the two agreeing well within one sigma. However, the calibration in equation (5) is to be preferred when comparing the secondary distance indicators presented in this paper, since it shares the same methodology used for TRGB, PNLf and GCLF.

To avoid uncertainties introduced by cluster depth effects, we prefer the direct calibration in equation (5) to a group calibration (such as the one adopted by Tonry et al. 1997), which would lead to a 0.1 mag (1σ) dimming of \overline{M}_I (based on the NGC 1023 group, the Fornax cluster, the Leo I group, the Virgo M87 and NGC 4472 subclusters, the NGC 5128 group, and the NGC 7331 group). On the downside, a direct calibration relies on the assumption of an identical stellar population in the bulges of the spiral calibrators and the ellipticals which are the main targets of the method. Additionally, as testified by the large error bars in the fluctuation magnitudes of bulges, SBF measurements in spirals are made difficult by the presence of dust and irregularities in the luminosity profile. The latter point is responsible for the larger dispersion shown in Figure 6 by the spirals compared to the ellipticals. In the lower part of the figure we follow Tonry et al. (1997) and fit all galaxies belonging to the five groups listed for five different zero points and a common slope. The solid points represent spiral galaxies in each group: given the admittedly limited amount of data, the spirals do not seem to occupy a different locus in the $[(V - I)_0, \overline{M}_I]$ plane compared to the ellipticals, which speaks in favor of a common \overline{M}_I for bulges and early-type galaxies. To illustrate the play of cluster depth effects, the upper part of Figure 6 shows the same galaxies but this time shifted vertically according to the mean Cepheid distance of the group to which they belong. Compared to the lower part of the figure, the points have now moved upwards (to fainter magnitudes) relative to the six spiral calibrators represented by the filled pentagons, due to galaxy type segregation in the clusters.

Based on the SBF and Cepheid distances, the elliptical and spiral populations in the Leo I group and the Fornax cluster have similar back-to-front extent: ~ 1 Mpc for the Leo I group and ~ 5 Mpc for the Fornax cluster. While the mean distance for both populations in Fornax is ~ 21 Mpc, the ellipticals in Leo I seem to be ~ 1 Mpc in the background of the spirals, which give a mean distance for the group of 10.5 Mpc. The situation is more complicated for the Virgo cluster. The ellipticals in the M87 and NGC 4472 subclusters show a fairly homogeneous distribution between 15 and 20 Mpc, with a mean close to 17 Mpc, while the Cepheid spirals show a significantly smaller back-to-front spread of less than 1 Mpc at a mean distance of 16 Mpc. Both SBF and Cepheid distances to the NGC 4649 subcluster do not support physical association for the galaxies in this region: SBF distances show a large back-to-front spread of 0.8 mag (~ 8 Mpc), while the Cepheid distance puts NGC 4639 at least 2 Mpc in the background of the region defined by the ellipticals.

6.2. *HST*/F814W SBF

Of the distance indicators presented in this paper, only F814W SBF has targeted galaxies beyond the 2000 km s^{-1} velocity range, which is of interest in the determination of the Hubble constant. A calibration of F814W SBF is therefore of great importance. The most recent calibration for F814W SBF is presented by Ajhar et al. (1997). The small sample size and the almost complete absence of overlap with Cepheid galaxies make it necessary to derive both zero points and slope of the color dependence of F814W SBF by comparison with the *I*-SBF distance moduli for the galaxies observed in both photometric bands. Using a sample of 16 galaxies with *I*-SBF distance moduli (Tonry et al. 1997, 1999), Ajhar et al. derive: $\overline{M}_{F814W} = (-1.73 \pm 0.07) + (6.5 \pm 0.7)[(V - I)_0 - 1.15] \text{ mag}$.

The galaxies in common between the F814W and *I*-SBF samples are listed in F99 and shown in Figure 7, where we have used equation (5) in calibrating the *I*-SBF magnitudes. Using a two-parameter fit, accounting for errors in both coordinates, gives $\overline{M}_{F814W} = (-1.91 \pm 0.10) + (7.4 \pm 1.2)[(V - I)_0 - 1.15] \text{ mag}$, and is shown by the dashed line in Figure 7. However, we prefer to adopt a different procedure than the one followed by Ajhar et al. (1997): the Kron-Cousin *I* and the WFPC2/F814W filters are not very dissimilar, and there is no reason to expect significant changes in the stellar population as seen in the two passbands. In fact, stellar population models (Worthey 1993, 1994) predict a slope of 4.3 for \overline{m}_I in the color range $1.05 < (V - I)_0 < 1.35$ (Blakeslee, Ajhar & Tonry 1999), close to the slope observed by Tonry et al. (1997). The same models applied to \overline{M}_{F814W} predict a virtually identical slope of 4.25 (Blakeslee, private communication). We conclude that the present amount of data is too limited to allow an empirical determination of the slope of the color dependence, and we prefer to impose the *I*-band slope of 4.5 ± 0.30 on \overline{M}_{F814W} (note that the error has been inflated compared to equation (5) to account for the 0.05 mag difference between the theoretical calibration in the two bands). This produces the fit shown by the solid line in Figure 7:

$$\overline{M}_{F814W} = [-1.70 \pm 0.10 \text{ (random)} \pm 0.16 \text{ (systematic)}] + (4.5 \pm 0.30)[(V - I)_0 - 1.15] \text{ mag} \quad (6)$$

As a consistency check, we also derived a magnitude zero point for F814W SBF using a comparison with Cepheid group distances for the Leo I group, the NGC 1023 group, and the M87 and NGC 4472 subclusters (the discrepant NGC 4649 subcluster has been excluded), after color correcting the F814W fluctuation magnitude using the slope given in equation (6). The resulting magnitude zero point, $-1.50 \pm 0.04 \text{ mag}$, is 2σ fainter than the one given by equation (6), confirming the importance of depth effects in deriving mean distances.

To conclude we must stress that the calibration of F814W SBF is likely to be significantly improved in the near future, when more F814W SBF measurements will be performed for galaxies in the *HST* public archive. In particular, it would be desirable to derive the slope of the color dependence using a large sample of galaxies belonging to different groups and clusters, as was

possible for I -SBF (Tonry et al. 1997).

7. Discussion of Distance Scales

7.1. Comparison of Secondary Distance Indicators

A summary of the magnitude zero points discussed in §3 through §6 is presented in Table 1, based on a direct (‘Gal’ in column 3), group (‘Group’) or mixed (‘Gal/Group’) comparison with the Cepheid distance moduli. The number of calibrators for each method is shown in column 2. Zero points are derived both assuming no metallicity dependence of the Cepheid PL relation (column 4) and a dependence as in Kennicutt et al. (1998) (column 5); the two sets of zero points will be compared in §7.2. Our final adopted zero points are underlined in the table. Applications of these zero points to the database of F99 gives the TRGB, PNLf, GCLF and SBF distances listed in Table 2. Distances derived from near infrared SBF measurements are followed by a colon to stress the fact that they are of limited reliability (see Appendix B). In Table 2, galaxies are grouped according to their cluster association, defined in F99. Column 2 gives the ‘membership index’ as in F99: galaxies which are certain, very likely, or just probable members of their assigned group or cluster are designated as class 1, 2, and 3 respectively. The last column in the table gives a weighted mean of all distances available to any particular galaxy, with the exclusion of GCLF, K_s and K' SBF. Heading each group of galaxies, is the cluster designation and the weighted mean of the cluster distances based on PNLf, GCLF, I -SBF, F814W-SBF and TRGB measurements to its members. In the case of I -SBF, more galaxies are averaged in the group distance than shown in the table. The full sample of galaxies can be found in Ajhar et al. (1999). Also noted in the table is the depth, in magnitudes, of each cluster, estimated based on the spatial extent of the cluster in the sky (see F99).

The only Cepheid calibrator in common to all secondary distance indicators is M31; therefore a comparison between the TRGB, PNLf, GCLF and I -SBF distance scales is not circular. Such a comparison is shown in Figures 8 and 9, and the results of a weighted least-squares fit to the data are summarized in Table 3.

Given the fact that the calibration of the V -band GCLF is rather uncertain, the only serious systematic effect emerging from Figures 8 and 9 is the discrepancy in zero points between the PNLf and SBF distance scales, also reported by Mendez (1998). We have tested for correlations between the distance moduli residuals and the galaxy color, as used in the SBF calibration, absolute B magnitude, T-type, and Mg_2 index, and found nothing of significance. Note that adopting a metallicity dependence of the Cepheid PL relation leading to larger distances to metal rich galaxies, as in Kennicutt et al. (1998), worsens the situation (see Table 1). A comparison between PNLf and Cepheid distance moduli (Figure 3 and Table 2) also shows a systematic offset between the local PNLf calibrators (which only extend as far as the Leo I group) and the Virgo and Fornax clusters. In a recent review, Jacoby, Ciardullo & Feldmeier (1998) found that PNLf

distances to Virgo ellipticals are, on average, 1.3 Mpc closer than Cepheid distances to Virgo spirals. Our study confirms Jacoby et al’s result, and it also shows a similar, but more pronounced trend for the Fornax cluster, the mean PNLF distance to which is 3.6 Mpc closer than measured by the Cepheids. This discrepancy is only partially reconciled if NGC 1425 is assumed to be in the background of the cluster: in this case the ellipticals with PNLF distances would be 1.8 Mpc closer than the two Cepheid spirals, NGC 1326A and NGC 1365.

There are several possibilities to explain the above observations. One is depth effects combined with Hubble type segregation in the Virgo and Fornax clusters. Indeed, Jacoby et al’s preferred explanation is that elliptical galaxies in the Virgo cluster are foreground with respect to the spirals. We do not favor this conclusion in view of the even larger PNLF–Cepheid discrepancy observed in the more compact Fornax cluster. Furthermore, PNLF and SBF distances *to the same early-type galaxies* in Virgo and Fornax are systematically offset by 0.3 mag, with the SBF galaxies giving mean cluster distances in better agreement with the Cepheids. A more likely cause of the observed systematics, in our opinion, is a bias in one, or more, of the PNLF, SBF or Cepheid distance scales.

While we cannot exclude Cepheids and SBF as being in error, three observations lead us to believe that PNLF is at least partially to blame: 1) as mention above, Cepheid and SBF distances agree for both the local sample and the Virgo and Fornax clusters, arguing that PNLF, rather than SBF or the Cepheids, is more likely affected by a systematic bias. 2) Recently, Mendez (1998) pointed out that contamination by intracluster PNe (stripped PNe that ‘float’ in the potential well of the cluster, but are not associated with any particular galaxy) could lead to an underestimate of the PNLF distances by up to 0.2 mag, particularly in moderately rich environments such as Virgo and Fornax. This effect acts in the same sense and is of the right order of magnitude to explain the PNLF/SBF and PNLF/Cepheid discrepancy. Because the Virgo and Fornax clusters in our sample also happen to be the richest ones, contamination of intracluster PNe would be more severe for these clusters than for the more nearby and smaller groups, as observed. 3) TRGB distance moduli agree well within 1σ with the SBF distance moduli, while the agreement with PNLF is marginally worse (1.5σ).

We have considered a few more possibilities that could lead to the observed systematic offsets, with no success. These include a metallicity dependence affecting the Cepheid distances, a possible corruption of the SBF measurements due to dust patches, stellar aggregates or globular clusters, and an inadequate corrections for Galactic reddening affecting both the PNLF and SBF distances. The metallicity dependence of the Cepheid PL relation has already been exonerated. The presence of dust or other contaminants in the SBF galaxies would lead to an overestimate of the fluctuation magnitudes, and thereby an underestimate of the distances, which is contrary to the observations. Because the Galactic extinction is practically the same within a particular cluster, if the amount of reddening in Virgo and Fornax had been overestimated this would artificially bring the PNLF distances closer, and the SBF distances further (because of the color dependence of the SBF calibration). However, even if the adopted DIRBE/IRAS reddenings are higher than the Burstein

& Heiles (1984) reddenings, adopting the latter would bring things into better agreement by no more than a few hundredths of a magnitude.

Finally, we tested for possible correlations between residuals of any combination of distance indicators and T-type, absolute B luminosity of the host galaxy, distance and environment (as given by the group velocity dispersion from Tully 1988), and found nothing of significance. In particular, this applies to previous claims of a dependence of the GCLF turnover magnitudes on environment and of the PNLFF cutoff magnitude on the B magnitude of the host galaxy (Figure 10), reported by Blakeslee & Tonry (1996) and Bottinelli et al. (1991) respectively. A Spearman rank-order correlation test gives a significance level consistent with the null hypothesis of no correlation within 1σ in both cases. Note that Blakeslee & Tonry’s claim was mainly motivated by published GCLF turnover measurements in Leo and Coma (Harris 1990, Baum et al. 1997). These measurements are not used in this paper, because they are based on GCLFs that do not adequately sample the turnover.

7.2. Effects of a Possible Metallicity Dependence of the Cepheid PL Relation

A review of the metallicity dependence of the Cepheid PL relation can be found in Kennicutt et al. (1998). To date, no agreement has been reached as to the magnitude of the change in the Cepheid distance modulus $(m - M)_0$ as a function of Cepheid metallicity $[O/H]$: some estimates which apply to Cepheid distances derived from V and I observations are $\delta(m - M)_0/\delta[O/H] < -0.1$ mag dex $^{-1}$ (Chiosi, Wood & Capitanio 1993), ~ -0.4 mag dex $^{-1}$ (Sasselov et al. 1997, Beaulieu et al. 1997, Kochanek 1997) and ~ -0.24 mag dex $^{-1}$ (Kennicutt et al. 1998), in the sense of increasing the distances of galaxies more metal rich than the LMC, which calibrates the Cepheid PL relation. However, recently Bono et al. (1999) derived $\delta(m - M)_0/\delta[O/H] \sim 0.75$ mag which acts in the *opposite* sense, i.e. decreasing the distance to galaxies more metal rich than the LMC. Because of the lack of consensus, in the previous sections we preferred to derive magnitude zero points for the secondary distance indicators applying no metallicity correction in the Cepheid PL relation. The magnitude of such correction can be judged from Figures 1 and 3–5, and Table 1 where we list magnitude zero points for both $\gamma = \delta(m - M)_0/\delta[O/H] = 0$, and $\gamma = -0.24$ mag dex $^{-1}$. While the effects of the metallicity dependence on the Cepheid distance to any single galaxy can be considerable, the repercussion on the calibration of secondary distance indicators is generally attenuated by having calibrators spanning a wide range in metallicities. Generally, galaxies with Cepheid distances outside the Local Group are large spirals more metal rich than the LMC. For example, the Cepheid distance to Fornax and Virgo increase by 0.05 and 0.15 mag respectively when a metallicity dependence as in Kennicutt et al. (1998) is assumed. Therefore, the calibration of PNLFF, GCLF and SBF, which is heavily weighted by galaxies outside the Local Group, will show a corresponding moderate dependence on the assumed metallicity dependence of the Cepheid PL relation, of the order of 0.05 to 0.10 mag for $\gamma = 0.24$ mag dex $^{-1}$. In contrast, with the exception of M31 and M33, all of the Local Group galaxies with Cepheid distances are

irregular systems slightly more metal poor than the LMC. The calibration of TRGB, which is based mainly on Local Group galaxies, shows a 0.05 change in zero point with metallicity, but in the opposite sense to that shown by PNLf, GCLF and SBF.

The data provided here can be used to check for systematic residuals versus Cepheid metallicity, as given by the $[O/H]$ indexes. Such a test performed using TRGB distances is particularly effective (Kennicutt et al. 1998). The correlation between TRGB – Cepheids distance moduli residuals and $[O/H]$ indexes is shown in Figure 11. The best weighted least-squares fit is consistent with a correlation at the 1.5σ level, and gives a slope of -0.18 ± 0.15 mag dex $^{-1}$. Bearing in mind that this test cannot be considered definitive, in view of the large error bars, the limited amount of data, and the lack of data points at high metallicities, this result is consistent with a metallicity dependence as in Kennicutt et al. (1998) and is smaller than predicted by Sasselov et al. (1997) and Beaulieu et al. (1997). While a similar test performed using I -SBF shows no significant correlation, the PNLf–Cepheids residuals correlate with the Cepheids $[O/H]$ indexes at the 2σ level, but in opposite sense than found above. This is unlikely due to a metallicity dependence of the PNLf distances (Jacoby & Ciardullo 1999), and we rather favor the conclusion of a spurious result, pinned by only one galaxy, NGC 3368, at the high metallicity end.

8. Addressing the Hubble Constant: Application of SBF

Of the distance indicators presented in this paper, F814W-SBF reaches far enough into the unperturbed Hubble flow to warrant its application in estimating the Hubble constant. Lauer et al. (1998) produced F814W-SBF measurements to the central galaxies in the Abell clusters A262, A3560¹⁶, A3565, and A3742, with heliocentric velocities between 3800 and 4900 km s $^{-1}$. An F814W fluctuation magnitude for NGC 4881 in the Coma cluster is published by Thomsen et al. (1997); however, the galaxy was not observed in the V band, and therefore the color dependence of the fluctuation magnitude cannot be calculated. Thomsen et al. estimate the amount of metallicity correction to \overline{M}_{F814W} based on a rather uncertain relation between \overline{m}_{F814W} and the Mg_2 index, calibrated using only one galaxy, NGC 3379. Finally, Pahre et al. (1999) present F814W-SBF measurements to NGC 4373 in the NGC 4373 group in the Hydra-Centaurus supercluster, at a heliocentric velocity of ~ 3400 km s $^{-1}$.

Reddenings, colors and fluctuation magnitudes for these galaxies are summarized in F99. For NGC 4881, we assumed the same color as for NGC 3379, since the two galaxies share the same Mg_2 index (Thomsen et al. 1997) and added a large error bar to incorporate the range of colors observed for early type galaxies in the SBF database: $(V - I)_0 = 1.2 \pm 0.1$. Distance moduli are calculated using the zero point given in equation (6), and the results are presented in Table 4.

¹⁶The galaxy observed by Lauer et al., attributed to Abell 3560, in reality belongs to a group at $cz = 3806$ km s $^{-1}$ in the foreground of the cluster. The actual Abell 3560 cluster is at a heliocentric velocity of ~ 15000 km s $^{-1}$ (Willmer et al. 1999).

The ~ 0.15 mag difference between our distance modulus for NGC 4373 and Pahre et al. is due mainly to differences in the Galactic extinction $E(B - V)$, our estimate being 0.03 mag smaller, and only marginally to the different SBF calibration. The distance moduli derived for the four Abell clusters are on average 0.3 magnitudes (1.5σ) larger than those derived by Lauer et al. (1998). Part of this difference is due to the calibration, and part to the fact that our adopted Schlegel et al. $E(B - V)$ reddenings are on average 0.03 magnitudes larger than the Burstein et al. values used by Lauer et al. Finally, the distance modulus to NGC 4881 in the Coma cluster is hardly significant because of the large uncertainty associated with the $(V - I)$ color; within the errors this distance is consistent with the value derived by Thomsen et al. (1997).

The last difficulty to overcome in our quest for H_0 is the determination of the clusters’ ‘cosmic’ velocities. We adopt velocities corrected for the local flow field as described in Mould et al. (1999). Briefly, the heliocentric velocities (column 6 of Table 4) are corrected first to the centroid of the Local Group using the prescription of Yahil, Tammann & Sandage (1977, listed in column 7 of Table 4; using other prescriptions, e.g. the IAU correction listed in column 8, does not produce a substantial difference), and then for infall towards three attractors, the contribution of which is assumed to be additive: Virgo, the Great Attractor (GA), and the Shapley Concentration. The flow-corrected velocities thus obtained are listed in column 10 of Table 4. For comparison we also list in column 6 of the same table the heliocentric systemic velocity of the cluster (from the CfA redshift Survey, Chen et al. 2000, see also <http://cfa-www.harvard.edu/~huchra/clusters>) and in column 9 the velocities in the reference frame defined by the cosmic microwave background (CMB), using the relation of Giovanelli et al. (1998) and a CMB dipole velocity as in Kogut et al. (1993). In three cases the differences between v_{flow} and v_{CMB} are larger than 10% of v_{CMB} . These are the clusters closest to the GA. These corrections make physical sense: the galaxies are moving towards the GA, and, the question is, how fast? The model is not capable of making accurate predictions close to the GA: linear infall is assumed, but here we are well inside the non-linear regime (Schechter 1980). Data exist on peculiar velocities for one of the three clusters, Abell 3560. Mould et al. (1991) find a peculiar velocity of 970 ± 420 km/sec. The model predicts 552 km s^{-1} . For these three clusters we regard the flow model’s predicted peculiar velocities as uncertain by $\pm (v_{CMB} - v_{flow})$ while for the remaining clusters we assume an error of 300 km s^{-1} following other papers in this series (Sakai et al. 1999, Gibson et al. 1999, Kelson et al. 1999).

The distance moduli and the flow-corrected velocities produce the values of H_0 listed in column 11 of Table 4 and plotted in Figure 12. A final value of H_0 is derived by fitting the Hubble diagram $v_{flow} = v_0 + H_0 * d$, with d equal to the distance to each individual cluster, by constraining the intercept $v_0 = 0$, and accounting for errors in both distances and velocities. This gives $H_0 = 70 \pm 4 \text{ km s}^{-1} \text{ Mpc}^{-1}$, where the error reflects only the 1σ uncertainty in the fit. Notice that a bivariate fit would not affect the value of H_0 and would give $v_0 = 75 \pm 1071 \text{ km/s}$, which justifies our imposed constraint of a zero intercept. The value of $H_0 = 70 \pm 4 \text{ km s}^{-1} \text{ Mpc}^{-1}$ is heavily weighted by the four Abell clusters; the Coma cluster and NGC 4373 carry little weight because of the large error bars in their distances and velocities respectively. Note that the four

Abell clusters yield H_0 that is 1σ lower than that derived from NGC 4373, possibly suggesting that the NGC 4373 group is in the foreground of the Hydra-Centaurus supercluster, onto which it projects.

Table 5 gives a summary of the contributions to the final uncertainty in the derived value of H_0 . Errors in the Cepheid distance scale have been reviewed extensively in all papers of this series; the current presentation differs only in the separation of systematic (identified by the letter S in Table 5) and random (R) contributions to the final error in the Cepheid distance to any individual galaxy. The errors in the SBF distance scale include the uncertainties in the photometric zero point and the extinction correction, which are described in Appendix A. Because the SBF fluctuation magnitudes are strongly dependent on color (equation 6), the error in the color-corrected F814W-SBF magnitudes includes not only the random errors in the fluctuation magnitudes (term 2.R₁), but also a term depending on the slope and error of the color dependence (4.5 ± 0.3). The color dependence of the SBF magnitudes produces typical errors of 4.5 times the error in the $(V - I)_0$ color (term 2.R₂), and 0.3 times $[(V - I)_0 - 1.15]$, added in quadrature. All of the above errors are random. The only source of systematic error is the zero point of the SBF calibration (term 2.S₁), ± 0.10 mag (§6.2). Note that random errors in the Cepheid PL calibration (R_{PL} in Table 5) are already accounted for in computing the error on the SBF zero point, and therefore need not be considered again. The systematic error on the Cepheid PL relation, however, has not yet been accounted for, and needs to be added in quadrature to term 2.S₁ to obtain the final systematic error on the F814W SBF distance scale of 0.19 magnitudes (S_{SBF}).

The error on the flow-corrected velocities (term 3.R₁) has been discussed already. Errors on H_0 are given by the formulae listed in the notes to part 3 of Table 5, for the case in which errors on the velocities and distances (d in Mpc) are identical for the N galaxies used to derive H_0 ; the generalization to the case in which the errors differ from object to object (as is our case) is straightforward.

In conclusion:

$$H_0 = 69 \pm 4(\text{random}) \pm 6(\text{systematic}) \text{ km s}^{-1} \text{ Mpc}^{-1}. \quad (7)$$

as determined using only the four Abell clusters. While we stress that a larger sample of SBF measurements is required with better sky coverage in order to reduce the propagation of the velocity flow model dependence into our estimate of H_0 , we notice that using CMB, rather than flow velocities, does not sensibly affect our result, producing $H_0 = 70 \pm 4 \text{ km s}^{-1} \text{ Mpc}^{-1}$ (random error only) as the weighted mean of the values obtained from the four Abell clusters. However, corrections for large scale flows are the largest cause of the difference between the value of H_0 above and the one derived by Tonry et al. (1999), $H_0 = 77 \pm 4 \pm 7 \text{ km s}^{-1} \text{ Mpc}^{-1}$. In particular, the Tonry et al. (1999) and Mould et al. (1999) flow models predict corrections of opposite sign for the velocities of two of the four Abell clusters considered in this paper, Abell 3560 and Abell 3565, due to a different placement of the Great Attractor. This alone produces a 5.5% increase in

H_0 when the Tonry et al. (1999) model is adopted. The remaining 5% increase is due equally to the adoption of a different zero point (see §6.1) and to the largest sample of clusters beyond 3000 km s⁻¹ available to Tonry et al. (1999). In passing, we will also point out that the difference between the value of H_0 derived in this paper and the one presented by Lauer et al. (1998, from the same Abell cluster used in our analysis) can be entirely ascribed to differences in the Galactic reddenings and the adopted SBF calibration.

Finally, the effects of a metallicity dependence of both the Cepheid PL relation, and the SBF magnitudes, need to be discussed. Assuming a metallicity dependence of the Cepheid PL relation as in Kennicutt et al. (1998) leads to a $\sim (5 \pm 3)\%$ decrease in H_0 (open circles in Figure 12). In §6.2, we derived a calibration of F814W SBF which differs from the original calibration of Ajhar et al. (1997) both in the zero point and in the slope of the color dependence. We also warned the reader that the latter is not well defined given the current set of calibrators. Fortunately, H_0 is not very sensitive to the slope of the color term in the calibration of F814 SBF, as long as this is accompanied by the appropriate change in zero point. For example, adopting Ajhar et al.’s slope would produce only a $\sim 1\%$ adjustment in H_0 .

9. Summary

We have derived a Cepheid calibration for four secondary distance indicators, applicable to the old stellar population in elliptical galaxies and the bulges and halos of spirals: the tip of the red giant branch method, the globular cluster luminosity function method, the planetary nebula luminosity function method and finally the surface brightness fluctuation method. GCLF and SBF data have been collected in more than one photometric band, namely V and B for the GCLF, and Kron-Cousins I , K_s , K' , and F814W for SBF, each of which was calibrated independently. TRGB, PNLF and I -SBF have been measured in a sufficient number of galaxies with Cepheid distances that their calibration can proceed through direct comparison for individual galaxies. However, the calibration of GCLF must proceed through a comparison of group, rather than individual distances, while the calibration of F814W SBF is better done against galaxies with I -SBF distances, calibrated in turn against the Cepheids.

Our derived zero points, summarized in Table 1, are improved compared to previously published values. This is not due only to the large dataset of Cepheid distances employed in this paper, but also, and perhaps mostly, to the homogeneity of the dataset used, both for the Cepheids and for the secondary distance indicators. While the Cepheids, TRGB and SBF distance scales show good agreement throughout the range of distances considered in this paper, distances derived using the PNLF method in the Virgo and Fornax clusters are systematically smaller (by ~ 0.35 mag) than given by either the SBF method or the Cepheids. A conclusion as to the significance of the discrepancy between PNLF and Cepheid distances is premature at this point, since it would require a knowledge of the spatial distribution of early and late type galaxies in the notoriously complex Virgo cluster. However, the difference between SBF and PNLF distances

measured *to the same galaxies* is real and needs to be solved with future work. Contamination of intracluster PNe, which leads to artificially overestimate the PNLF cutoff magnitudes especially in richer clusters such as Virgo and Fornax, acts in the correct sense, but is probably not sufficient, to correct the observed discrepancy.

We also found a large scatter in the distances derived using the GCLF method, pointing to the existence of a second parameter affecting the GCLF turnover magnitude. At present, we estimate the GCLF turnover magnitude to be uncertain by 0.25 mag and 0.5 mag in the V – and B –bands respectively.

We studied the correlation of residuals of TRGB and Cepheid distances against $[O/H]$ indices as a test of the metallicity dependence of the Cepheid PL relation. Our results are consistent with the findings of Kennicutt et al. (1998) using Cepheid distances in two fields of M101, and both are consistent with no metallicity dependence of the Cepheid PL relation. For PNLF and SBF, the effects of a metallicity dependence of the Cepheid PL relation as in Kennicutt et al. (1998) acts in the sense of brightening the magnitude zero points by about 0.10 magnitudes, due to the fact that most of the calibrating galaxies are metal rich.

We have applied our newly derived calibration to calculate F814W-SBF distances to four Abell clusters with group velocities in the 4000 km s^{-1} range, using the data by Lauer et al. (1998). By adopting a velocity flow model from Mould et al. (1999) to correct the cluster velocities for large scale flows, we obtain a value for the Hubble constant of $H_0 = 69 \pm 4(\text{random}) \pm 6(\text{systematic}) \text{ km s}^{-1} \text{ Mpc}^{-1}$. We find that this result is insensitive (at the 1% level) to the slope of the metallicity dependence of the F814W SBF fluctuation magnitude, however, a metallicity dependence of the Cepheid PL relation as in Kennicutt et al. (1998) will lower the Hubble constant by $(5 \pm 3)\%$.

We wish to thank John Tonry, John Blakeslee, Ed Ajhar and Alan Dressler for kindly giving us access to the SBF database prior to publication. Many thanks also to John Blakeslee, John Tonry, George Jacoby, Pat Côté and Pat Durrell for helpful discussions. LF acknowledges support by NASA through Hubble Fellowship grant HF-01081.01-96A awarded by the Space Telescope Science Institute, which is operated by the Association of Universities for Research in Astronomy, Inc., for NASA under contract NAS 5-26555. The work presented in this paper is based on observations with the NASA Hubble Space Telescope, obtained by the Space Telescope Science Institute. Support for this work was also provided by NASA through grant GO-2227-87A from STScI. This research has made use of the NASA/IPAC Extragalactic Database (NED), version 2.5 (May 27, 1998). NED is operated by the Jet Propulsion Laboratory, California Institute of Technology, under contract with the National Aeronautics and Space Administration.

A. Uncertainty in the Extinction Corrections

Uncertainties in the extinction corrections contribute to the final error in the dereddened magnitudes through: 1) the uncertain definition of the extinction curve itself $k(\lambda - V) = E(\lambda - V)/E(B - V)$; 2) errors in the assumed value of R_V ; and 3) errors in the adopted value of the foreground $E(B - V)$. In terms of the three quantities above, $A_\lambda = (K(\lambda - V) + R_V) \times E(B - V)$; therefore, the error on the extinction corrected magnitude is:

$$\sigma_{m_\lambda}^2 = \sigma_{E(B-V)}^2 \times (A(\lambda)/E(B - V))^2 + E(B - V)^2 \times \sigma_{k(\lambda-V)}^2 + E(B - V)^2 \times \sigma_{R_V}^2 \quad (8)$$

Similarly, $E(\lambda - V) = k(\lambda - V) \times E(B - V)$; therefore, errors in the colors are given by

$$\sigma_{m(\lambda-V)}^2 = \sigma_{E(B-V)}^2 \times k(\lambda - V)^2 + E(B - V)^2 \times \sigma_{k(\lambda-V)}^2. \quad (9)$$

For wavelengths longwards of 4000 Å, $\sigma_k(\lambda - V) \sim 0$ (Fitzpatrick 1999); therefore, the second term in the equations above drops out. The uncertainty in $E(B - V)$ is given as ± 0.015 mag for the Burstein and Heiles (1984) reddenings, and 16% for the DIRBE/IRAS maps (Schlegel et al. 1998). Finally, we adopt $\sigma_{R_V} = 0.3$. Note that for typical values of $E(B - V) \sim 0.1$, σ_{m_λ} amounts to ~ 0.05 magnitudes at V and I wavelengths.

B. The Calibration of K_s and K' SBF

SBF measurements in the K' and K_s bands do not comprise a sufficiently large sample size or have the required accuracy to determine the dependence of the SBF absolute magnitude on metallicity. Zero points have been determined using galaxies in common with I -SBF surveys by Pahre & Mould (1994) as $\overline{M}_{K_s} = -5.74 \pm 0.18$ (based on a sample of seven Virgo galaxies, plus NGC 3379, M31 and M32, the latter two observed in the K' band) and Jensen, Tonry & Luppino (1998) as $\overline{M}_{K'} = -5.61 \pm 0.12$ (based on a sample of Virgo, Fornax and Eridanus galaxies, plus M31 and M32).

Because a satisfactory overlap is not present with Cepheid galaxies, the calibration of both K_s and K' SBF magnitudes must proceed through I -SBF. Assuming the calibration given in equation (5) for I -SBF, we derive $\overline{M}_{K_s} = -6.01 \pm 0.11$ and $\overline{M}_{K'} = -5.77 \pm 0.11$ using DIRBE/IRAS reddenings, and assuming no metallicity dependence of the Cepheid PL relation. NGC 4489 shows large residuals from the mean in K_s datasets, and has therefore been rejected from the fit. Following Jensen et al. (1998), we have also rejected NGC 1339, NGC 1395, NGC 1400, NGC 1426, NGC 4489 and NGC 4578 from the calibration of K' . The difference between our calibration and the ones from Pahre & Mould (1994) and Jensen, Tonry & Luppino (1998) are due to the

different magnitude zero point adopted for I -SBF, the switch to DIRBE reddenings, and revision to the published I fluctuation magnitudes (Tonry et al. 1999).

We must stress that a final calibration of the near-infrared SBF must await a larger dataset (Jensen et al. 1998), in particular the dependence of the fluctuation magnitude on color should be empirically determined. Figure 13 shows the color dependence of the fluctuation magnitudes given the available data. Formal fits give slopes of -8.3 ± 4.6 in K_s and $+5.0 \pm 0.8$ in K' , however it is rather obvious that these estimates cannot be reliable in view of the fact that the slopes are expected to be similar in the two passbands.

C. Magnitude Zero Points Using HI Reddenings

Magnitude zero points for TRGB, PNLf, GCLF and SBF, derived as in §3–§6, but using HI rather than DIRBE/IRAS reddenings, are given in Table 6. In no cases are the differences significant. Note that, because HI reddenings are systematically smaller than the DIRBE/IRAS reddenings, the effect of adopting them is to make the zero points for PNLf, TRGB and GCLF fainter by a few hundredth of a magnitude. The effect on SBF is opposite, i.e. the zero points become brighter, due to the color dependence of the SBF calibration (§6).

REFERENCES

- Abraham, R. G., & van den Bergh, S. 1995, *ApJ*, 438, 218
- Ajhar, E. A., et al. 1997, *AJ*, 114, 626
- Ajhar, E. A., et al. 1999, in preparation
- Arce, H. G. & Goodman, A. A. 1999, *ApJL*, 512, 135
- Ashman, K. M., Conti, A., & Zepf, S. E. 1995, *AJ*, 110, 1164
- Baum, W., et al. 1995, *AJ*, 110, 2537
- Baum, W., et al. 1997, *AJ*, 113, 1483
- Beaulieu, J. P., et al. 1997, *A&A*, 318, L47
- Blakeslee, J.P., & Tonry, J.L. 1996, *ApJL*, 465, L19
- Blakeslee, J. P., Ajhar, E. A., & Tonry, J. L. 1999, in ‘Post-Hipparcos Cosmic Candles’, eds. A. Heck & F. Caputo, Kluwer Academic Publishers, p.181
- Böhringer, H., et al. 1994, *Nature*, 368, 828
- Bono, G., Caputo, F., Castellani, V., & Marconi, M 1999, *ApJ*, 512, 711
- Bothun, G. D., Harris, H. C., & Hesser, J. E. 1992, *PASP*, 104, 1220
- Bottinelli, L., Gouguenheim, L., Paturel, G., & Teerikorpi, P. 1991, *A&A*, 252, 550
- Burstein, D., & Heiles, C. 1984, *ApJS*, 54, 33
- Cardelli, J. A., Clayton, G. C. & Mathis, J. S. 1989, *ApJ*, 345, 245
- Chen, J., Huchra, J., McNamara, B., Mader, J. 2000, in preparation.
- Chiosi, C., Wood, P. R., & Capitanio, N. 1993, *ApJS*, 86, 541
- Ciardullo, R., & Jacoby, G.H. 1992, *ApJ*, 388, 268
- Ciardullo, R., Jacoby, G.H., Feldmeier, J. J., & Bartlett, R. E. 1998, *ApJ*, 492, 62
- Ciardullo, R., Jacoby, G.H., Ford, H. C., & Neill, J. D. 1989, *ApJ*, 339, 53
- Da Costa, G. S., & Armandroff, T. E. 1990, *AJ*, 100, 162
- Della Valle, M., Kissler-Patig, M., Danziger, J., & Storm, J. 1998, *MNRAS*, 299, 267
- Dopita, M. A., Jacoby, G. H., & Vassiliadis, E. 1992, *ApJ*, 389, 27
- Elson, R. A. W., & Santiago, B. X. 1996, *MNRAS*, 280, 971
- Feldmeier, J., Ciardullo, R., & Jacoby, G.H., 1997, *ApJ*, 479, 231
- Ferguson, H. C., Tanvir, N. R., & von Hippel, T. 1998, *Nature*, 391, 461
- Ferrarese, L., et al. 1996, *ApJ*, 464, 568
- Ferrarese, L., et al. 1998, *ApJ*, 507, 655
- Ferrarese, L., et al., 1999, *ApJS*, submitted (F99)

- Fitzpatrick, E. L. 1999, *PASP*, 111, 63
- Forbes, D. 1996, *AJ*, 112, 1409
- Ford, H.C., et al. 1996, *ApJ*, 458, 455
- Freedman, W. L. et al. 1994, *ApJ* 427, 628
- Freedman, W. L., Mould, J. R., Kennicutt, R. C., & Madore, B. F. 1998, *astro-ph/9801080*
- Frogel, J. A., Persson, S. E., & Cohen, J. G. 1983, *ApJS*, 53, 713
- Gavazzi, G., Boselli, A., Scodreggio, M., Pierini, D., & Belsole, E. 1999, *MNRAS*, 304, 595
- Gibson, B., et al. 1999, *ApJ*, submitted
- Giovanelli, R., et al. 1998, *ApJL*, 505, 91
- Goudfrooij, P., de Jong, T., Hansen, L., & Norgaard-Nielsen, H.U. 1994, *MNRAS*, 271, 833
- Grillmair, C. J., Forbes, D. A., Brodie, J., & Elson, R. 1999, *AJ*, 117, 167
- Harris, W. E., Durrell, P. R., Pierce, M. J., & Secker, J. 1998, *Nature*, 395, 48
- Harris, W. 1990, *PASP*, 102, 966
- Harris, W. 1991, *ARA&A*, 29, 543
- Harris, W., Allwright, J., Pritchett, C., & van den Bergh, S. 1991, *ApJS*, 76, 115
- Holtzman, J. A. et al. 1995, *PASP*, 107, 1065
- Jacoby, G. H. 1996, *The Extragalactic Distance Scale*, Proceedings of the ST ScI May Symposium, Eds.: M. Livio, M. Donahue, and N. Panagia, Cambridge University Press, p. 197
- Jacoby, G. H., Ciardullo, R., and Feldmeier, J. J. 1998, in *ASPC 167, Harmonizing Cosmic Distance Scales in a Post-Hipparcos Era*, eds. D. Egret & A. Heck, p. 175.
- Jacoby, G. H., et al. 1992, *PASP*, 104, 599
- Jacoby, G. H., Ciardullo, R., & Ford, H.C. 1990, *ApJ*, 356, 332
- Jacoby, G. H., & Ciardullo, R. 1999, *ApJ* 515, 169
- Jacoby, G. H., Ciardullo, R., & Harris, W.E. 1996, *ApJ*, 462, 1
- Jacoby, G. H., Walker, A.R., & Ciardullo, R. 1990, *ApJ*, 365, 461
- Jensen, J. B., Tonry, J. L., & Luppino, G. A. 1998, *ApJ*, 505, 111
- Jensen, J. B., et al. 1999, *BAAS*, 194, 5102
- Jerjen, H., Freeman, K. C., & Binggeli, B. 1998, *AJ*, 116, 2873
- Kelson, D., et al. 1999, *ApJ*, submitted
- Kennicutt, R. C., Freedman, W. L., & Mould, J. R. 1995, *AJ*, 110, 1476
- Kennicutt, R. et al. 1998, *ApJ*, 498, 181
- Kochanek, C. S. 1997, *ApJ*, 491, 13

- Kogut, A., et al. 1993, ApJ, 419, 1
- Kundu, A., & Whitmore, B. C. 1998, AJ, 116, 2841
- Kundu, A., et al. 1999, ApJ, 513, 983
- Kurucz, R. L. 1979, ApJS, 40, 1
- Lauer, T. R., Tonry, J. L., Postman, M., Ajhar, E. A., & Holtzman, J. A. 1998, ApJ, 499, 577
- Lauer, T. R., & Postman, M. 1992, ApJ, 400, L47
- Lee, M. G., Freedman, W.L., & Madore, B.F. 1993, ApJ, 417, 552
- Madjesky, R., & Rabolli, M. 1995, A&A, 297, 660
- Madore, B. F. & Freedman, W. L. 1991, PASP, 103, 933
- Madore, B. F., Freedman, W. L., & Sakai, S. 1996, The Extragalactic Distance Scale, Proceedings of the ST ScI May Symposium, Eds.: M. Livio, M. Donahue, and N. Panagia, Cambridge University Press
- McMillan, R., Ciardullo, R., & Jacoby, G.H. 1993, ApJ, 416, 62
- Mendez, R. H. 1998, Proceedings of the meeting Post-Hipparcos Cosmic Candles, eds. A. Heck & F. Caputo, Kluwer Academic Publishers, p.161
- Mould, J. R., et al. 1991, ApJ, 383, 467
- Mould, J.R., et al. 1999, ApJ, submitted
- Pahre, M. A., & Mould, J. R. 1994, ApJ, 433, 567
- Pahre, M. A., et al. 1999, ApJ, 515, 79
- Rieke, G. H., & Lebofsky M. J. 1985, ApJ, 288, 618
- Sakai, S. 1999, in ‘Cosmological Parameters and the Evolution of the Universe’, IAU Symposium no. 183, Kyoto, Japan, ed. K. Sato, Dordrecht, Boston : Kluwer Academic, p. 48
- Sakai, S., et al. 1997, ApJ, 478, 49
- Sakai, S., et al. 1999, ApJ, submitted
- Salaris, M., & Cassisi, S. 1998, MNRAS, 298, 166
- Salaris, M., & Cassisi, S. 1996, A&A, 305, 858
- Sandage, A., & Tammann, G. 1995, ApJ, 446, 1
- Sandage, A., & Tammann, G. 1996, ApJL, 464, 51
- Sasselov, D., et al. 1997, A&A, 324, 471
- Schechter, P. L. 1980, AJ, 85, 801
- Schlegel, D. J., Finkbeiner, D. P., & Davis, M. 1998, ApJ, 500, 525
- Schultz, G.V., & Wiemer, W. 1975, A&A, 43, 133

- Secker, J. 1992, *AJ*, 104, 1472
- Stanghellini, L. 1995, *ApJ*, 452, 515
- Thomsen, B., Baum, W.A., Hammergren, M. & Worthey, G. 1997, *ApJ*, 483, L37
- Tonry, J. L., & Schneider, P. 1988, *AJ*, 96, 807
- Tonry, J.L, Blakeslee, J.P., Ajhar, E.A. & Dressler, A. 1997, *ApJ*, 475, 399
- Tonry, J. L., Blakeslee, J. P., Ajhar, E.A., & Dressler, A. 1999, *astro-ph/9907062*
- Tully, R. B. 1988, in *Nearby Galaxies Catalog*, Cambridge and New York, Cambridge University Press.
- West, M, Côté, P., Jones, C., Forman, W., Marzke, R. O. 1995, *ApJL*, 453, 77
- Whitmore, B. 1996, *The Extragalactic Distance Scale*, Proceedings of the ST ScI May Symposium, Eds.: M. Livio, M. Donahue, and N. Panagia, Cambridge University Press, p. 254
- Whittet, D. C. B., & van Breda, I. G. 1980, *MNRAS*, 192, 467
- Willmer, C. N. A. 1999, *astro-ph/9906023*
- Worthey, G. 1993, *ApJ*, 409, 530
- Worthey, G. 1994, *ApJS*, 95, 107
- Yahil, A., Tammann, G. A., & Sandage, A. 1977, *ApJ*, 217, 903

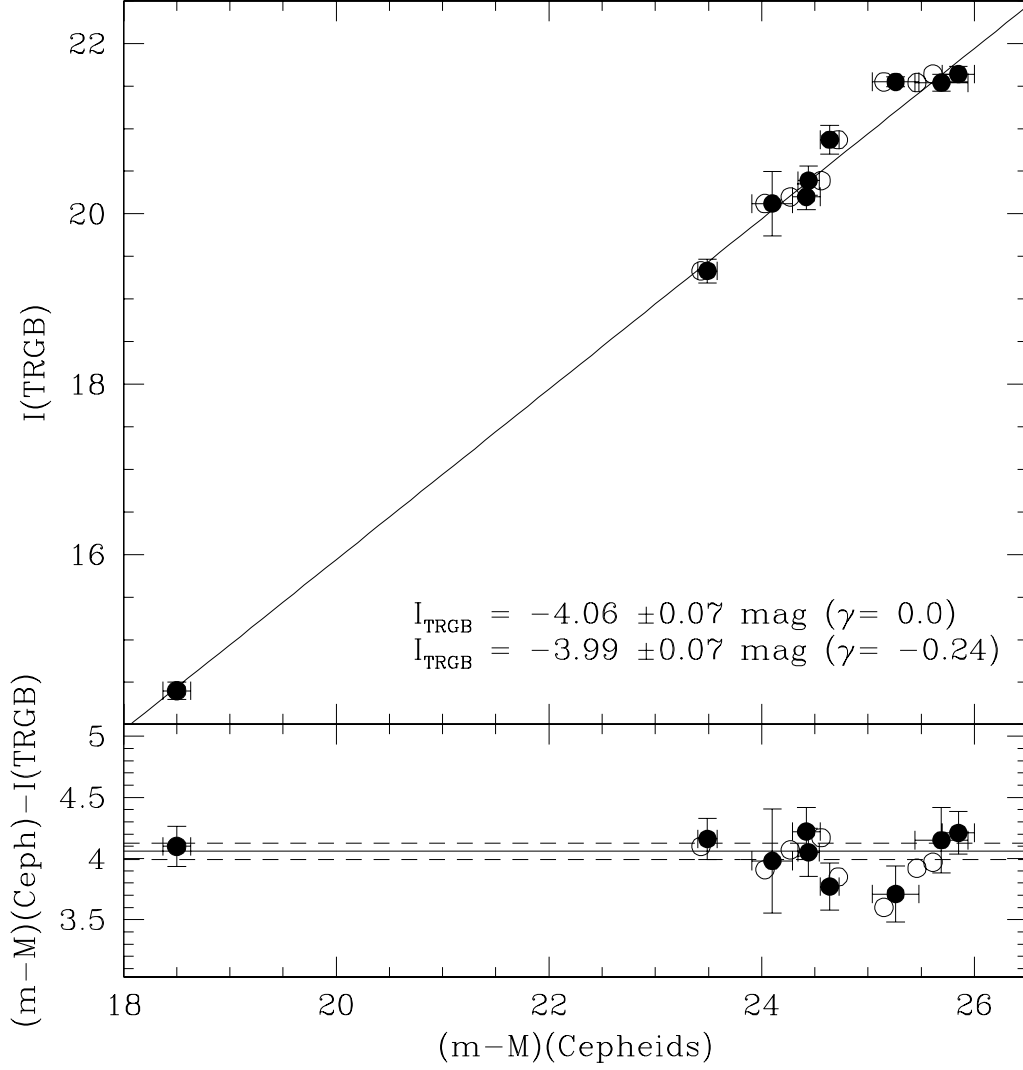


Fig. 1.— Zero point calibration for the TRGB method, based on a galaxy by galaxy comparison. In this and all subsequent figures, all magnitudes have been corrected for extinction using DIRBE/IRAS reddenings and the extinction coefficients given in §2. Filled circles assume no dependence of the PL relation on metallicity: the solid line in the upper panel shows the best fitting line, assuming a fixed slope of 1.0, and determined considering errors in both variables. The same line, and the 1σ uncertainty of the mean, is shown in the lower panel, where residuals are plotted. Small open circles assume a metallicity dependence as in Kennicutt et al. (1998, $\gamma = \delta(m - M)_0 / \delta[O/H] = -0.24$, the error bars are comparable to the previous case). The zero points and 1σ errors are listed in the figure for both of the assumed metallicity dependences. The galaxies are, from left to right: LMC, NGC 6822, IC 10, IC 1613, M31, M33, NGC 3109, Sextans B and Sextans A.

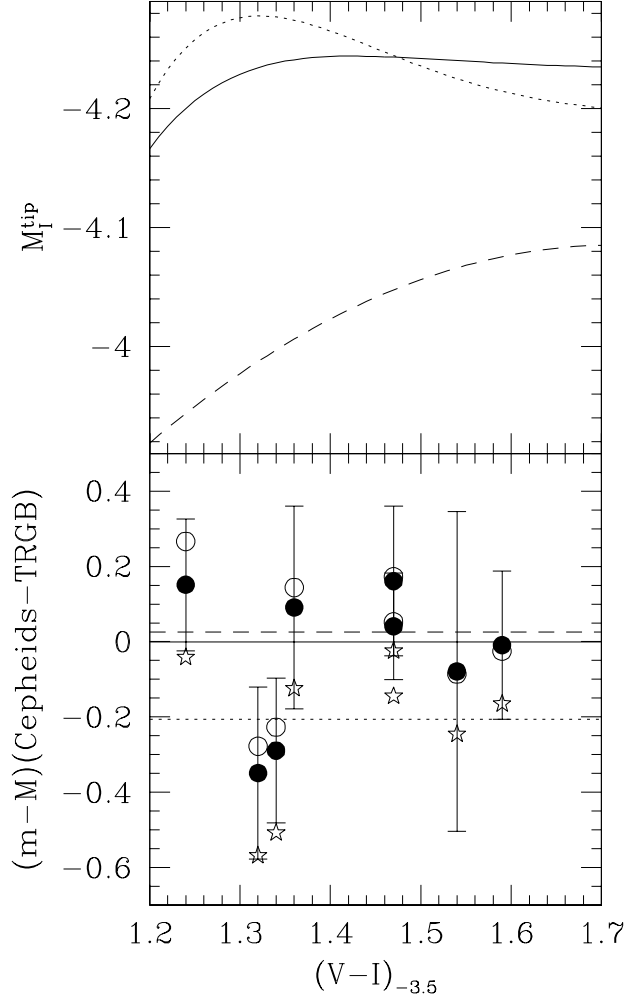


Fig. 2.— The top panel shows the color dependence of the absolute I magnitude of the TRGB predicted by Lee et al. (1993, dashed line) and Salaris and Cassisi (1998, the dotted and solid lines use Kurucz’ stellar models and Yale isochrones respectively). The lower panel shows the Cepheid – TRGB distance moduli residuals using: the calibration given in equation (1) (solid dots and error bars); the Lee et al. calibration (open circles, with a mean shown by the dashed line); the Salaris & Cassisi calibration (stars, with a mean given by the dotted line). The galaxies are, from left to right: Sextans A, NGC 3109, NGC 598, Sextans B, LMC, IC 1613, IC 10, and NGC 224. NGC 6822 is not plotted since its $(V-I)_{-3.5}$ color places it outside the range of metallicities considered by the primary calibration.

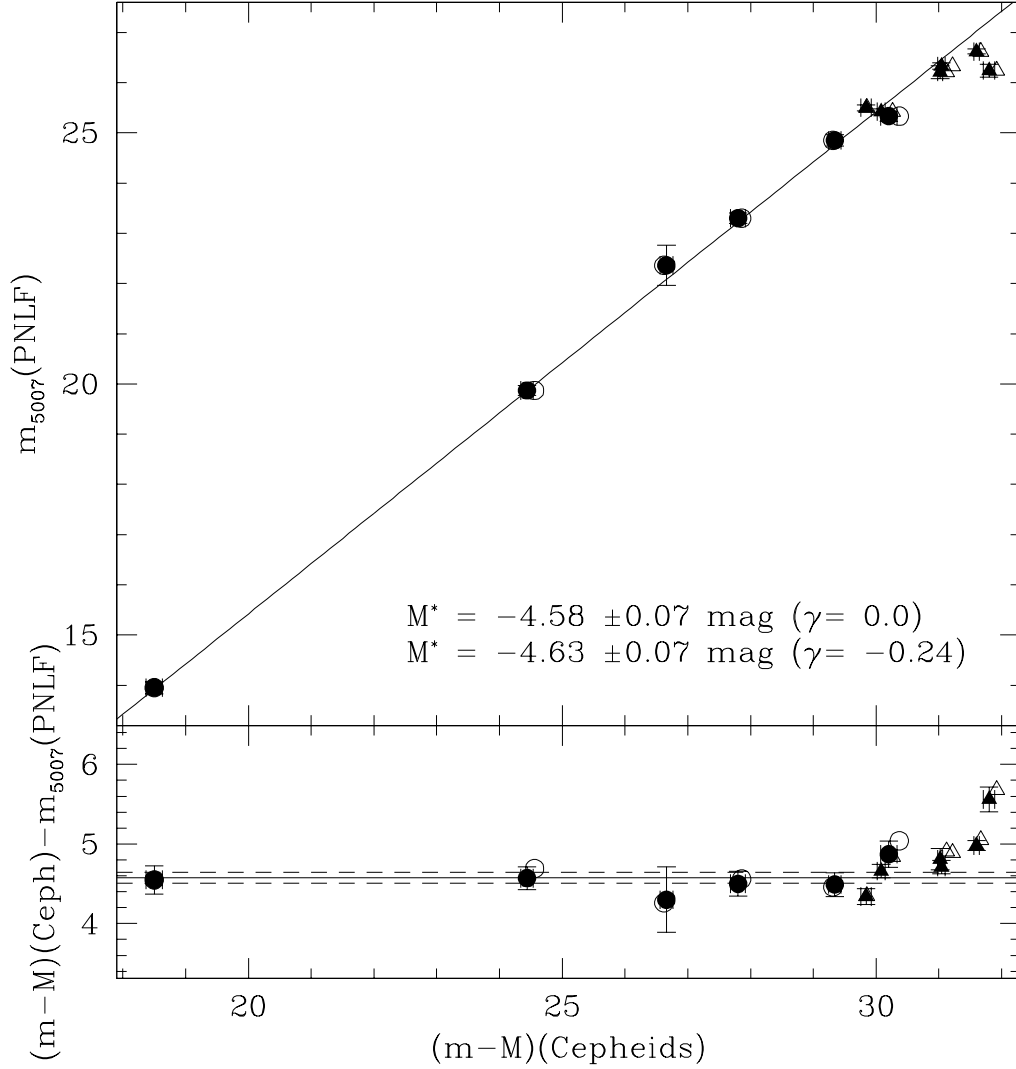


Fig. 3.— Direct zero point calibration for the planetary nebula luminosity function method, based on galaxy comparison with the Cepheids. Shown in the figure are the calibrator galaxies (circles) and also for comparison group distances and mean PNLf cutoff magnitudes (triangles). The filled and open symbols refer to the degree of metallicity dependence as in Figure 1. The galaxies are, from left to right: LMC, M31, NGC 300, M81, M101 and NGC 3368. The groups are: NGC 1023 Group, the Leo I group, the NGC 4472 subcluster, the M87 subcluster, Fornax and the NGC 4649 subcluster. The fits leading to the magnitude zero points listed in the figure are performed using only the six galaxies.

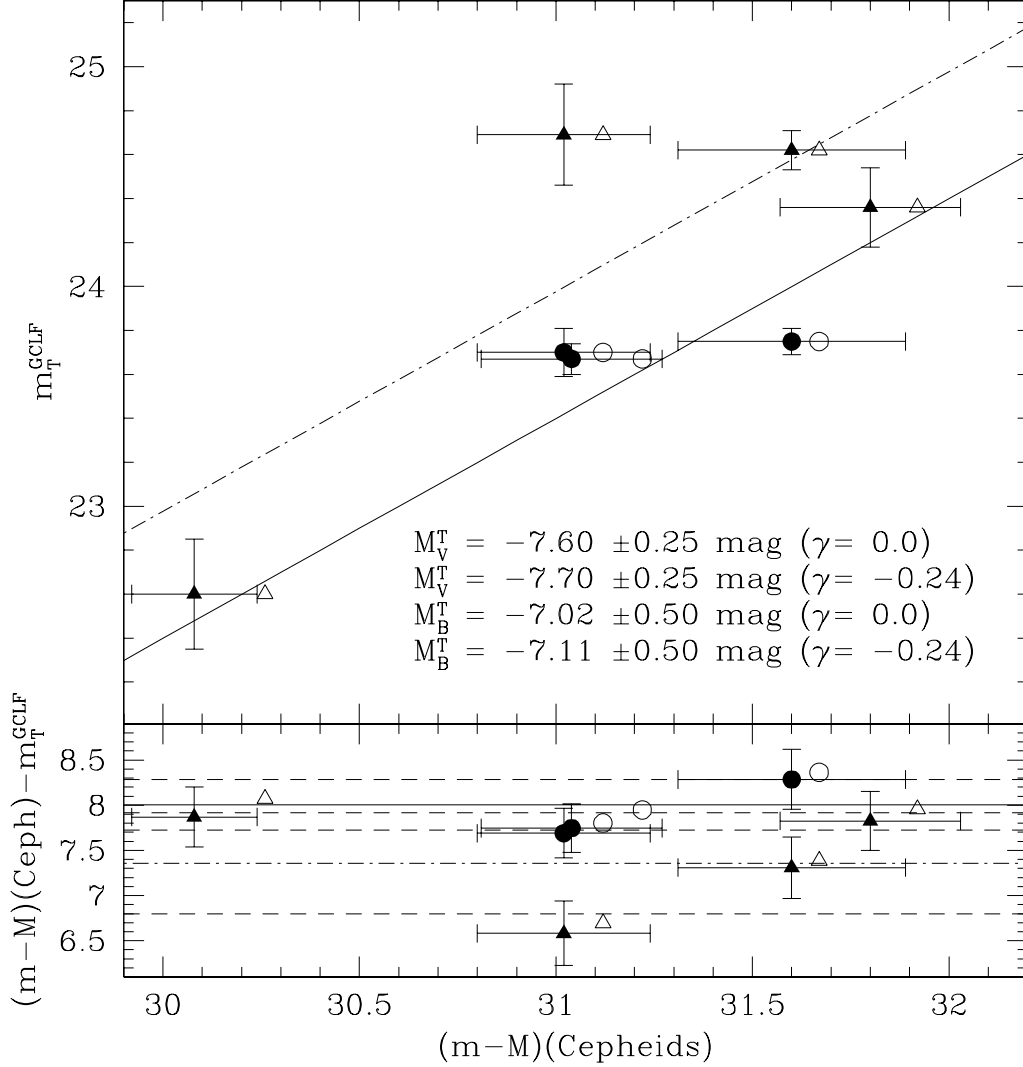


Fig. 4.— Zero point calibration for the V -band (circles) and B -band (triangles) GCLF methods, based on a group by group comparison with the Cepheids. Filled and open symbols refer to the degree of metallicity dependence of the Cepheid PL relation, as in Figure 1. The groups are, from left to right: V -band GCLF: the NGC 4472 subcluster, the M87 subcluster, and Fornax cluster; B -band GCLF: Leo I group, the NGC 4472 subcluster, Fornax and the NGC 4649 subcluster. Formal fits are shown by the solid line for the V -band GCLF and by the dot-dashed line for the B -band GCLF.

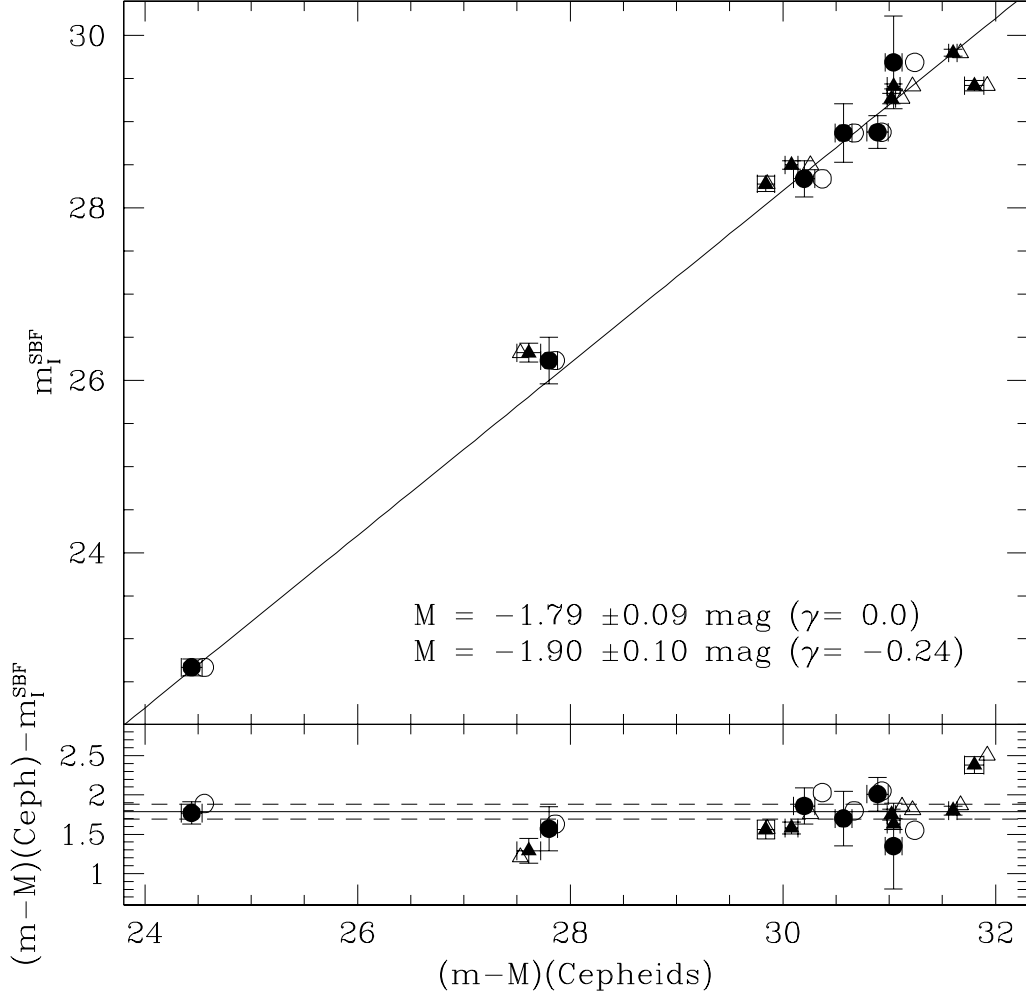


Fig. 5.— Zero point calibration for the *I*-SBF method, based on a direct comparison of galaxies with Cepheid distances and SBF fluctuation magnitudes. A color correction has been applied to the SBF magnitudes as described in §6. For comparison, both galaxies (circles) and clusters (triangles) are plotted in the figure. The filled and open symbols refer to the degree of metallicity dependence as in Figure 1. The galaxies are, from left to right: M31, M81, NGC 3368, NGC 4725, NGC 7331 and NGC 4548. The groups are the NGC 5128 group, NGC 1023 group, Leo I group, the M87 and NGC 4472 subclusters, Fornax cluster and the NGC 4649 subcluster.

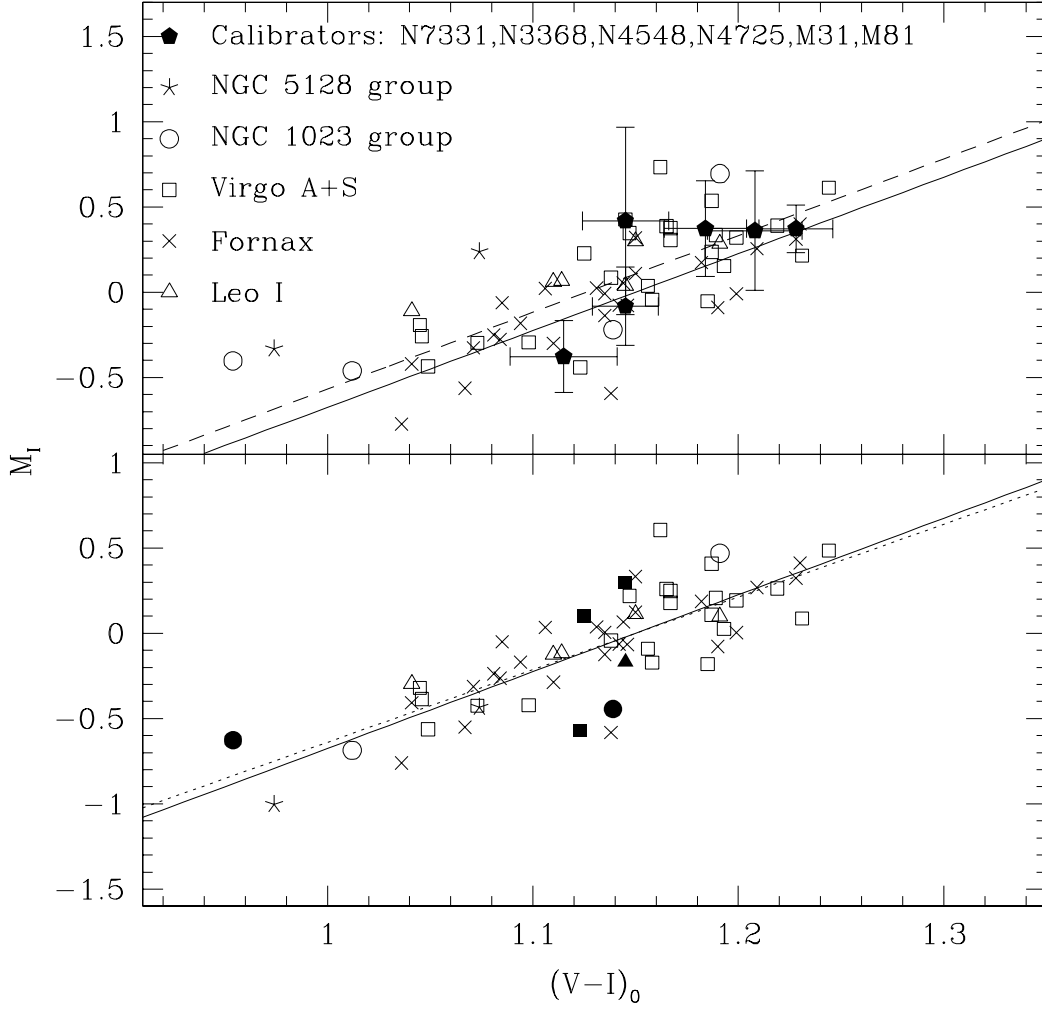


Fig. 6.— In the lower panel are plotted galaxies belonging to the groups identified in the top left, shifted vertically according to their mean magnitude at $(V-I)_0 = 1.15$, following Tonry et al. (1997). The open and filled symbols refer to elliptical and spiral galaxies respectively. The solid line has a slope of 4.5, as in Tonry et al. (1997), while the dotted line is our best fit to the data. In the top panel the galaxies are shifted vertically according to the mean Cepheid distance of the group to which they belong. The Cepheid galaxies on which our SBF calibration (shown by the solid line) is based are shown by the solid pentagons. A calibration based exclusively on group distances is shown by the dashed line.

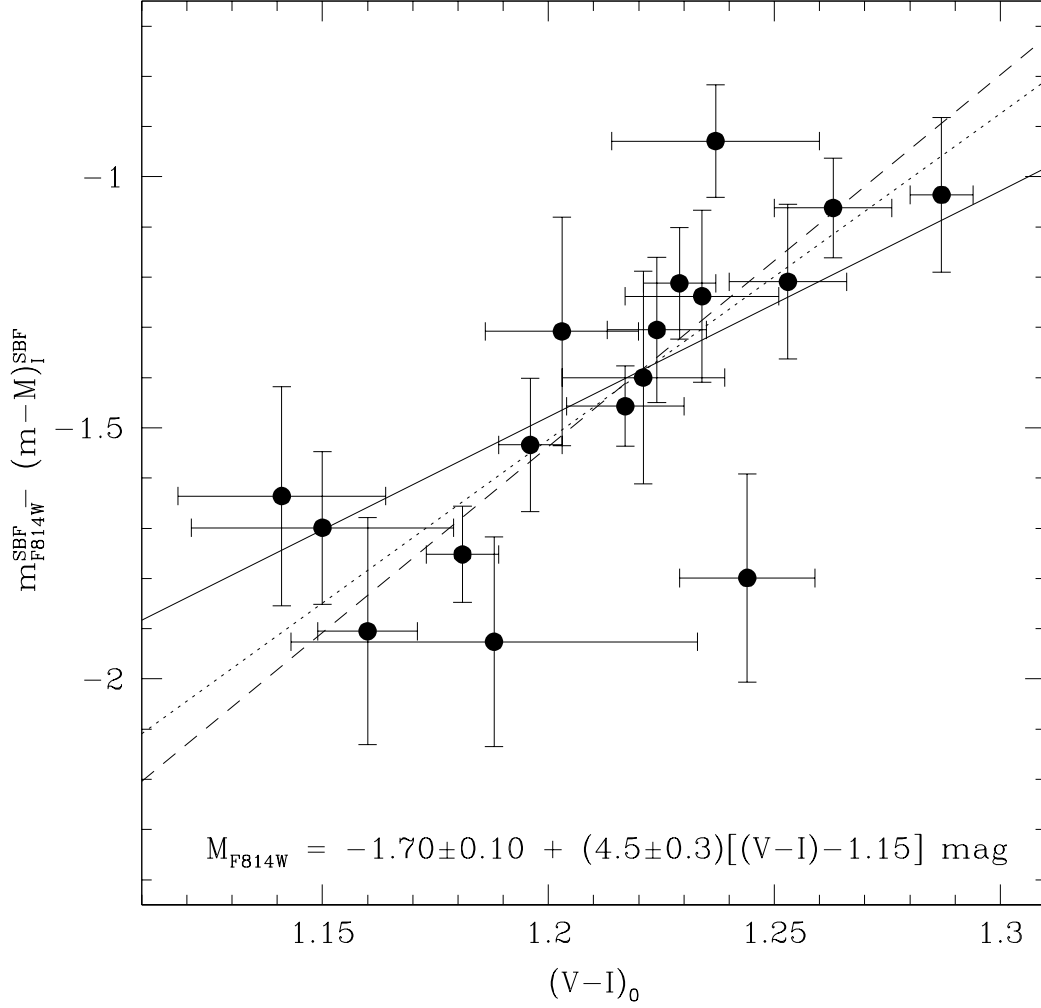


Fig. 7.— Tertiary calibration for the F814W-SBF method, calibrated against the *I*-SBF method. The lines are as follows. Solid line: our adopted best fit which assumes a 4.5 slope, as in equation (6); dotted line: fit with an assumed slope of 6.5 as in Ajhar et al. (1997); dashed line: unconstrained fit (both slope and zero point). M31 is the point at (1.237, −0.936).

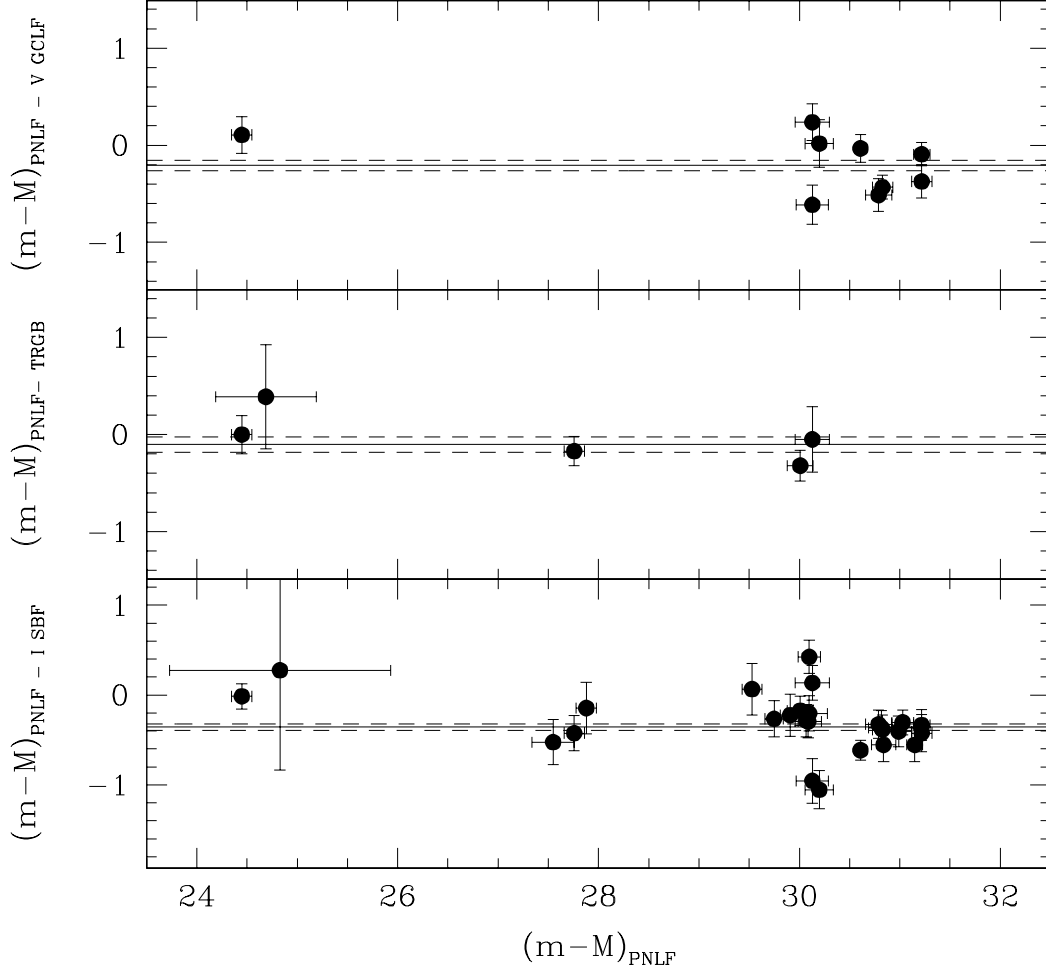


Fig. 8.— Comparison between galaxy distance moduli derived using the PNLF method and the I -SBF, TRGB and V -GCLF methods, calibrated as in Table 1. The solid and dashed lines are the best fit to the galaxy data points and the 1σ deviations respectively.

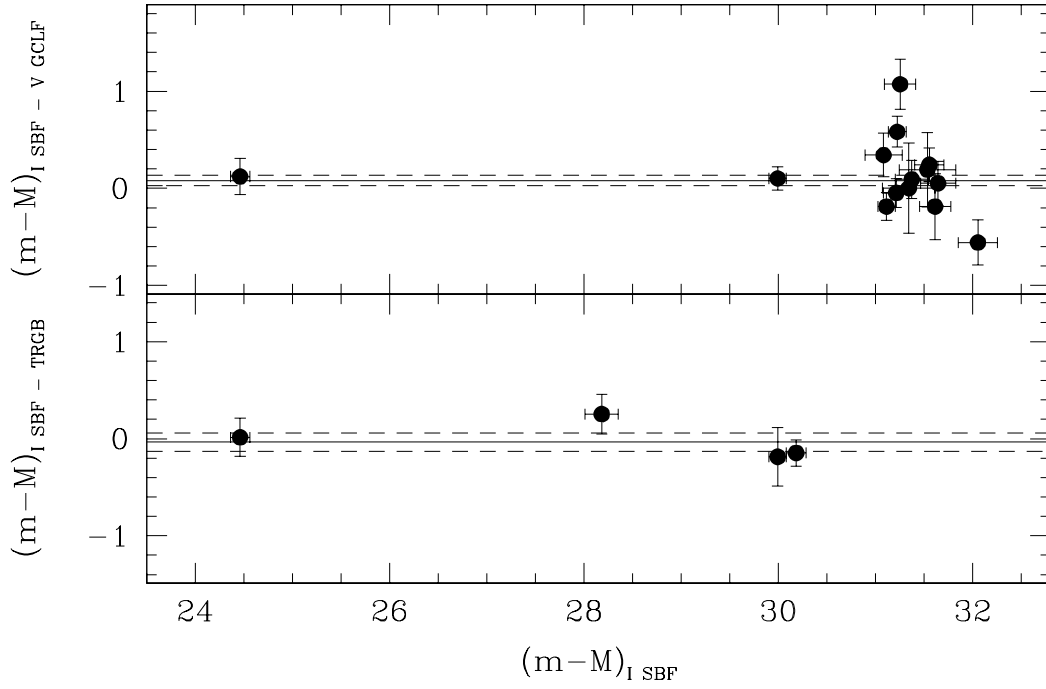


Fig. 9.— Comparison between galaxy distance moduli derived using the I -SBF method and the TRGB and V -GCLF methods, calibrated as in Table 1. The solid and dashed lines are the best fit to the galaxy data points and the 1σ deviations respectively.

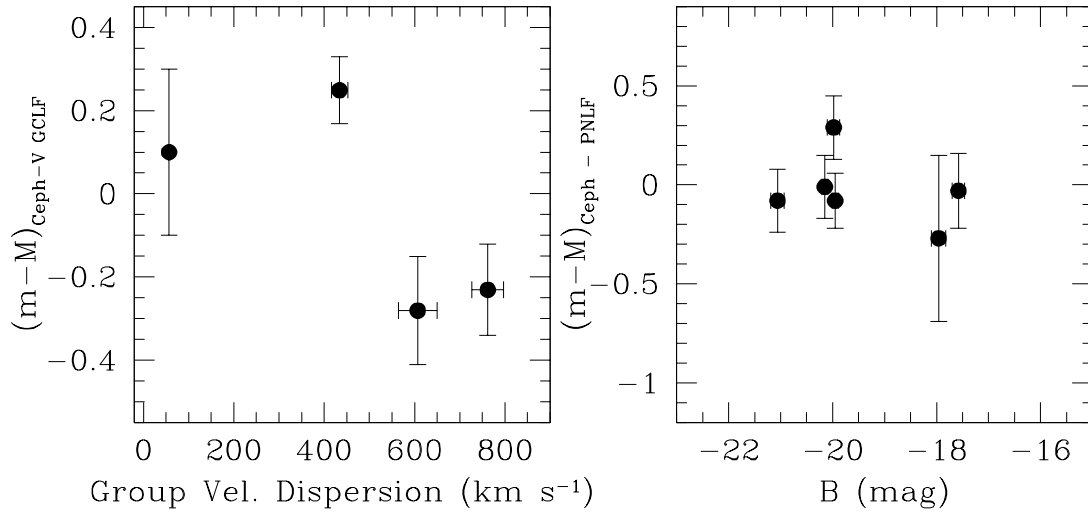


Fig. 10.— Cepheid- V GCLF and Cepheid-PNLF distance moduli residuals plotted against the cluster velocity dispersion and of the absolute B magnitude of the host galaxy respectively.

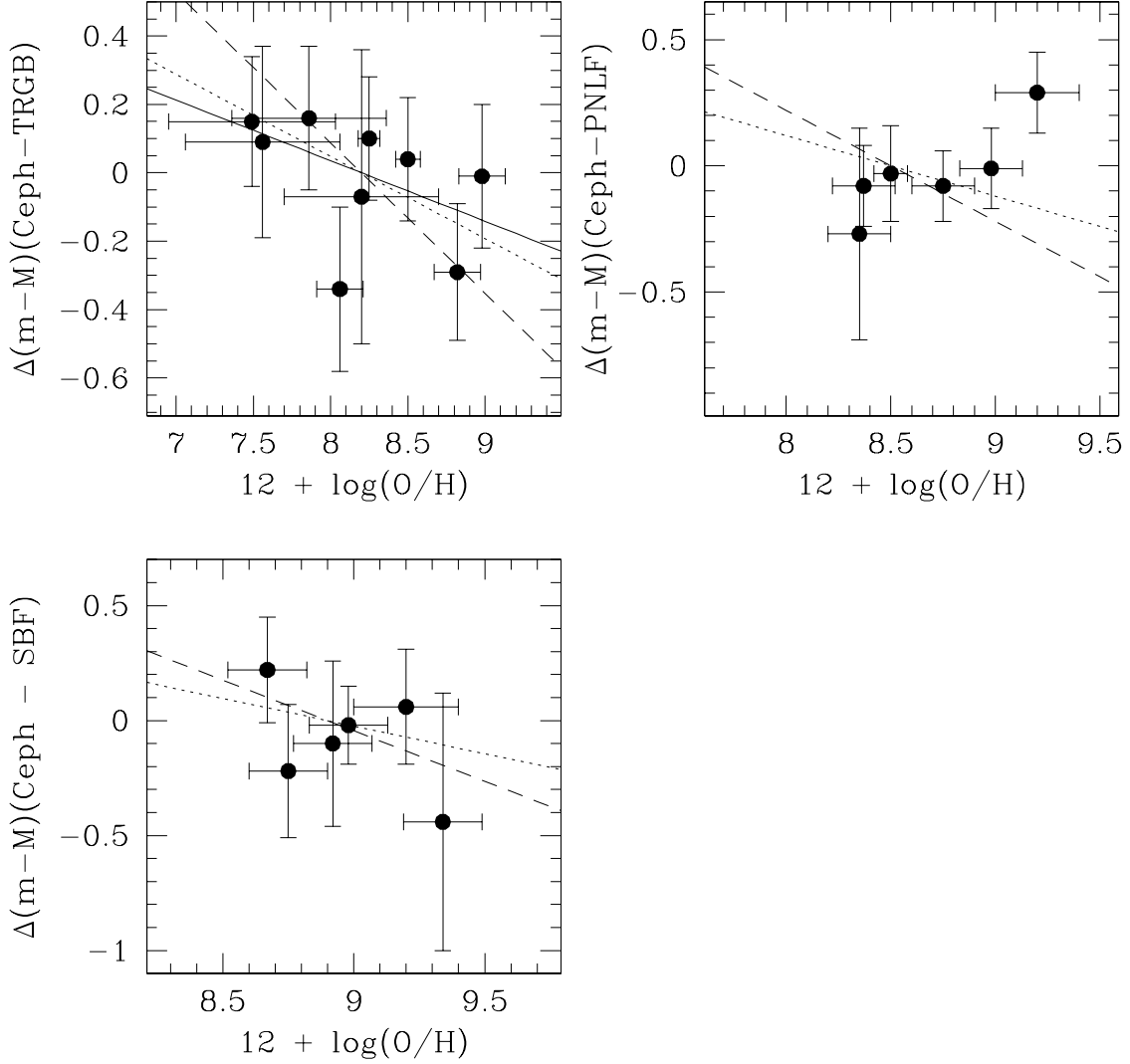


Fig. 11.— Test for the metallicity dependence of the Cepheid PL relation. Cepheids abundances are plotted in the x-axis. The solid line is a bivariate fit to the data points. The dotted lines show the relation expected based on the metallicity dependence of the Cepheid PL relation derived by Kennicutt et al. (1998). The dashed lines show the relation expected given the metallicity dependence of Sasselov et al. (1997) and Beaulieu et al. (1997).

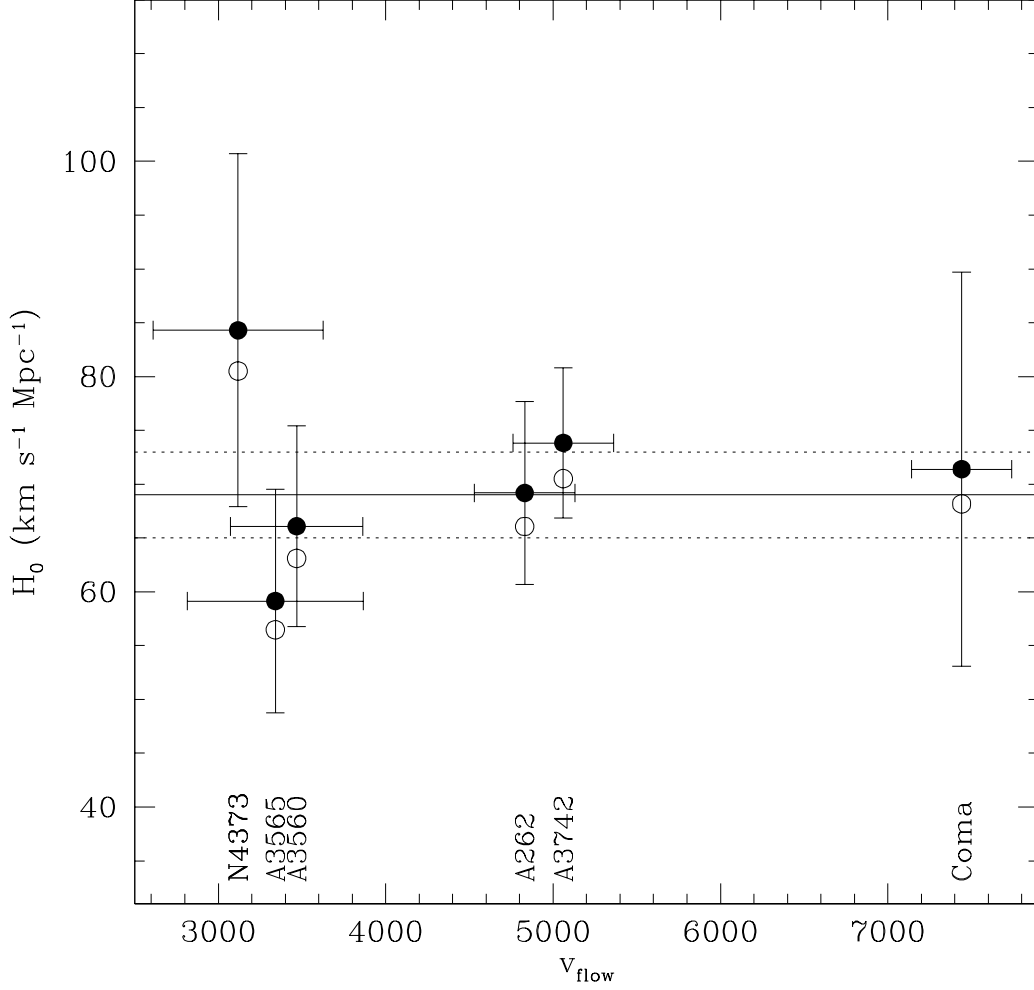


Fig. 12.— Values of the Hubble constant, H_0 , derived from *HST*/WFPC2/F814W-SBF distances, calibrated as described in §6. Group velocities are corrected for a flow model (see text for further details). The solid and open points assume no metallicity dependence for the Cepheid PL relation, and a metallicity dependence as in Kennicutt et al. (1998) respectively. The solid and dotted lines give the weighted mean and 1σ error of the values of H_0 derived for the four Abell clusters, assuming no metallicity dependence of the Cepheid PL relation.

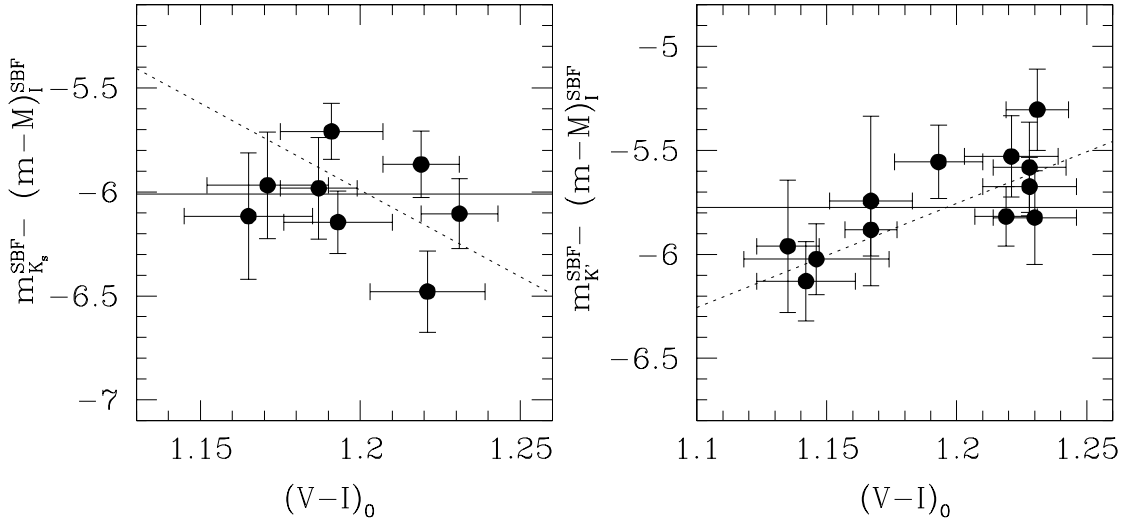


Fig. 13.— Color dependence of the near infrared SBF method. Formal bivariate fits to the data give slopes of -8.3 ± 4.6 in K_s and 5.0 ± 0.8 in K' , shown by the dotted lines. Our adopted zero points, assuming no color dependence, are shown by the solid lines.

Table 1. Calibration of Secondary Distance Indicators

Indicator	No.	Gal/ Group ¹	Zero Point ² $\gamma=0.00$	Zero Point ³ $\gamma = -0.24 \pm 0.16$	Notes
TRGB	9	Gal	<u>-4.06 ± 0.07</u> (0.80)	-3.99 ± 0.07 (0.63)	
	4	Gr	-4.00 ± 0.05 (4.03)	-4.11 ± 0.06 (6.07)	
PNLF	6	Gal	<u>-4.58 ± 0.07</u> (0.83)	-4.63 ± 0.07 (1.60)	
	10	Gr+Gal	-4.61 ± 0.06 (0.83)	-4.68 ± 0.06 (1.40)	
V GCLF	3	Gr	<u>-7.60 ± 0.25</u> (12.0)	-7.70 ± 0.25 (7.98)	
	1	Gal	<u>-7.70 ± 0.19</u> (N/A)	-7.82 ± 0.19 (N/A)	4
B GCLF	4	Gr	<u>-7.02 ± 0.50</u> (5.48)	-7.11 ± 0.50 (6.03)	
I SBF	6	Gal	<u>-1.79 ± 0.09</u> (0.51)	-1.90 ± 0.10 (0.43)	5
	6	Gr	-1.69 ± 0.03 (2.87)	-1.79 ± 0.03 (3.25)	5
F814W-SBF	17	Gal	<u>-1.70 ± 0.10</u> (1.38)	-1.81 ± 0.10 (1.38)	6,7
	4	Gr	-1.50 ± 0.04 (4.19)	-1.63 ± 0.04 (6.70)	7

¹‘Gal’ denotes a direct calibration based on a galaxy-by-galaxy comparison, ‘Gr’ denotes a calibration based on group distances, ‘Gal+Gr’ denotes a mixed calibration based both on group and galaxy distances. Unless noted, all calibrations are based on Cepheid distances. Details for each indicators can be found in the text and accompanying figures. Cluster depth effects are included in the errors on the group distances for the mixed calibration, but not for the calibration based exclusively on groups.

²Derived assuming no metallicity dependence of the Cepheid PL relation. The error is the 1σ uncertainty in the fit, see §3–6 for an estimate of the systematic uncertainties. The numbers in parentheses represent the reduced χ^2 of the fit. Our adopted final magnitude zero points are underlined in the table.

³Derived assuming a metallicity dependence of the Cepheid PL relation as in Kennicutt et al. (1998).

⁴Based on a direct comparison for M31 only.

⁵The calibration assumes a color dependence of the fluctuation magnitudes as in equation (5).

⁶Calibrated against the *I*-SBF distances, calibrated as in equation (5).

⁷The calibration assumes a color dependence as in equation (6).

TABLE 2 IS IN LANDSCAPE FORMAT, THEREFORE IN A SEPARATE FILE

Table 3. Comparisons of Secondary Distance Indicators

Indicators	$\Delta \pm \sigma$ Difference ^a (mag)
PNLF – TRGB	-0.12 ± 0.08
PNLF – SBF	-0.36 ± 0.04
PNLF – <i>V</i> GCLF	-0.22 ± 0.05
<i>I</i> SBF – TRGB	-0.03 ± 0.09
<i>I</i> SBF – <i>V</i> GCLF	$+0.08 \pm 0.05$

^aWeighted mean of the difference in the distance moduli derived using galaxies in common between the two distance indicators listed in the first column. The sigma represents the rms error in the mean.

TABLE 4 IS IN LANDSCAPE FORMAT, THEREFORE IN A SEPARATE FILE

Table 5. Error Budget

	Source	Error ¹	Notes
1.	ERRORS ON THE CEPHEID DISTANCE SCALE		
	<i>A. LMC True Modulus</i>	± 0.13	
	<i>B. LMC PL Zero Point</i> ²	± 0.02	
S _{1.1}	LMC PL Systematic Error	± 0.13	A and B added in quadrature
	<i>C. HST V-Band Zero Point</i> ³	± 0.03	
	<i>D. HST I-Band Zero Point</i> ³	± 0.03	
S _{1.2}	Systematic Error in the Photometry	± 0.09	$\sqrt{C^2(1-R)^2 + D^2R^2}$, $R = A(V)/E(V-I)$
R _{1.1}	Random Error in the Photometry	± 0.05	From DoPHOT/ALLFRAME comparison
	<i>E. R_V Differences Between Galaxy and LMC</i>	± 0.014	See Ferrarese et al. (1998) for details
	<i>F. Error in the adopted value for R_V</i>	± 0.01	See Appendix A for details
R _{1.2}	Random Error in the Extinction Treatment	± 0.02	E and F added in quadrature
	<i>G. PL Fit (V)</i>	$\pm 0.05^4$	
	<i>H. PL Fit (I)</i>	$\pm 0.04^4$	
R _{1.3}	Random Error in the Cepheid True Modulus ⁵	$\pm 0.06^4$	G and H partially correlated.
R _{PL}	Total Random Error	$\pm 0.08^4$	R _{1.1} , R _{1.2} and R _{1.3} added in quadrature
S _{PL}	Total Systematic Error	± 0.16	S _{1.1} and S _{1.2} added in quadrature
2.	ERRORS ON THE F814W-SBF DISTANCE SCALE		
	<i>A. Error on the Reddened SBF Magnitudes</i>	$\pm 0.10^4$	see F99
	<i>B. Error on the Reddened Colors</i>	$\pm 0.02^4$	see F99
	<i>C. Error on the $A(F814W)$ Extinction</i>	$\pm 0.03^4$	See Appendix A for details
	<i>D. Error on the $E(V-I)$ reddening</i>	$\pm 0.01^4$	See Appendix A for details
R _{2.1}	Random Error on the SBF Magnitudes	$\pm 0.10^4$	A and C added in quadrature
R _{2.2}	Random Error on the Colors	$\pm 0.02^4$	B and D added in quadrature
R _{2.3}	Random Error on the Color Corrected Mag.	$\pm 0.15^4$	$\sqrt{R_{2.1}^2 + (4.5R_{2.2})^2 + (0.3((V-I)_0 - 1.15))^2}$
S _{2.1}	Systematic Error on the Zero Point	± 0.10	From Table 1, R _{PL} already folded in
R _{SBF}	Total Random Error	$\pm 0.15^4$	R _{2.3}
S _{SBF}	Total Systematic Error	$\pm 0.19^4$	S _{2.1} and S _{PL} added in quadrature
3.	ERRORS ON H_0		
R _{3.1}	Random Error on the Flow Velocities	$\pm 400^4$	in km s ⁻¹
R _{H₀}	Total Random Error on H_0 (km/s/Mpc)	± 4	$\sqrt{(R_{3.1}/d)^2 + (0.46H_0R_{SBF})^2}/\sqrt{N}$
S _{H₀}	Total Systematic Error on H_0 (km/s/Mpc)	± 6	$0.46H_0S_{SBF}$

¹Errors in 1. and 2. are in magnitudes, and as indicated in 3.

²Equal to the scatter around the dereddened PL relation for the LMC (± 0.12 mag) divided by the square root of the number of LMC Cepheids, 32 (Madore & Freedman 1991).

³Contributing uncertainties from the Holtzman et al. (1995) zero points, and the ‘long versus short’ uncertainty, combined in quadrature.

⁴The values quotes are typical of the galaxies observed, but individual cases vary slightly. See the individual references for the correct values of specific galaxies.

⁵The partially correlated nature of the derived PL width uncertainties is taken into account by the (correlated) de-reddening procedure, coupled with the largely ‘degenerate-with-reddening’ positioning of individual Cepheids within the instability strip.

Table 6. Final Zero Points Using HI Reddenings

Indicator	Zero Point ¹	Δ^2	Notes
TRGB	-4.03 ± 0.07 (0.72)	-0.02	Galaxy calibration via Cepheids
PNLF	-4.53 ± 0.07 (1.00)	-0.05	Galaxy calibration via Cepheids
<i>V</i> GCLF	-7.57 ± 0.25 (10.8)	-0.03	Group calibration via Cepheids
<i>B</i> GCLF	-6.96 ± 0.50 (5.50)	-0.06	Group calibration via Cepheids
<i>I</i> -SBF	-1.84 ± 0.10 (0.41)	$+0.04$	Galaxy calibration via Cepheids
F814W-SBF	-1.73 ± 0.11 (0.99)	$+0.02$	Galaxy calibration via <i>I</i> -SBF, calibrated as above
<i>K'</i> -SBF	-5.75 ± 0.11 (1.85)	-0.03	as above
<i>K_s</i> -SBF	-6.01 ± 0.13 (1.54)	-0.01	as above, excluding NGC 4489

¹Derived assuming no metallicity dependence of the Cepheid PL relation. The error is the 1σ uncertainty in the fit, see §3–6 for an estimate of the systematic uncertainties. The numbers in parentheses represent the reduced χ^2 of the fit.

²Difference between the magnitude zero points derived using DIRBE/IRAS (from Table 1) and HI reddening.

Table 2. Final Cepheid, TRGB, PNLf, GCLF, & SBF Distance Moduli¹

Galaxy	Class ²	$(m - M) \pm \sigma$ Cepheids ³	$(m - M) \pm \sigma$ TRGB ³	$(m - M) \pm \sigma$ PNLF ³	$(m - M) \pm \sigma$ V-GCLF ³	$(m - M) \pm \sigma$ B-GCLF ³	$(m - M) \pm \sigma$ I-SBF ^{3,4}	$(m - M) \pm \sigma$ F814W-SBF ³	$(m - M) \pm \sigma$ K_s -SBF ³	$(m - M) \pm \sigma$ K' -SBF ³	$(m - M) \pm \sigma$ MEAN ⁵
Local Group											
AndV	1	...	24.66±0.13	24.66±0.13
AndVI	1	...	24.61±0.12	24.61±0.12
GR8	1	≤26.8:
IC10	1	24.10±0.19	24.17±0.39	24.11±0.17
IC1613	1	24.42±0.13	24.26±0.16	24.36±0.10
LeoI	1	...	21.99±0.12	21.99±0.12
LeoA	1	...	24.52±0.21	24.52±0.21
LeoB	1	...	21.73±0.21	21.73±0.21
LGS3	1	...	24.58±0.21	24.58±0.21
LMC	1	18.50±0.13	18.46±0.12	18.53±0.14	18.49±0.07
N205	1	...	24.30±0.21	24.68±0.51	24.36±0.20
N221	1	24.83±1.10	24.55±0.17	24.56±0.17	...	24.31:±0.14	24.56±0.17
N224	1	24.44±0.10	24.45±0.19	24.45±0.13	24.34±0.30	...	24.46±0.14	24.84±0.15	...	24.56:±0.14	24.51±0.06
N598	1	24.64±0.09	24.93±0.18	24.70±0.08
N3109	1	25.26±0.22	25.60±0.09	≤26.26:±0.41	25.56±0.08
N6822	1	23.49±0.09	23.39±0.16	23.47±0.08
SextansA	1	25.85±0.15	25.70±0.11	25.76±0.09
SextansB	1	25.69±0.25	25.60±0.12	25.62±0.11
SMC	1	18.99±0.05	...	19.29:±0.31	18.99±0.05
WLM	1	...	24.84±0.12	24.84±0.12
N1023 Group	1	29.84±0.08	...	30.08±0.08	30.08±0.11	30.44±0.14	30.03±0.05
Depth 0.32 mag											
N891	1	30.10±0.13	29.67±0.18	29.95±0.10
N925	1	29.84±0.08	29.84±0.08
N1023	1	30.07±0.11	30.35±0.19	30.44±0.14	30.23±0.08
Fornax Cluster	1	31.60±0.04	...	31.20±0.07	31.38±0.15	31.76±0.31	31.59±0.04	31.51:±0.08	31.52±0.03
Depth 0.28 mag											
N1316	1	31.15±0.11	31.71±0.19	31.28±0.09
N1326A	1	31.43±0.07	31.43±0.07
N1339	1	31.66±0.37	31.73:±0.18	31.66±0.37
N1344	1	31.34±0.35	...	31.53±0.31	31.35:±0.16	31.53±0.31
N1365	1	31.39±0.10	31.39±0.10
N1379	1	31.92±0.58	31.56±0.17	31.21:±0.17	31.56±0.17
N1380	1	31.28±0.27	...	31.37±0.20	31.37±0.20
N1399	1	31.22±0.11	31.31±0.27	31.56±0.51	31.56±0.17	31.75:±0.19	31.31±0.09

Table 2—Continued

Galaxy	Class ²	$(m - M) \pm \sigma$ Cepheids ³	$(m - M) \pm \sigma$ TRGB ³	$(m - M) \pm \sigma$ PNLF ³	$(m - M) \pm \sigma$ V-GCLF ³	$(m - M) \pm \sigma$ B-GCLF ³	$(m - M) \pm \sigma$ I-SBF ^{3,4}	$(m - M) \pm \sigma$ F814W-SBF ³	$(m - M) \pm \sigma$ K_s -SBF ³	$(m - M) \pm \sigma$ K' -SBF ³	$(m - M) \pm \sigma$ MEAN ⁵
N1404	1	31.22±0.12	31.59±0.29	31.85±0.54	31.64±0.20	31.59±0.18	31.33±0.10
N1425	1	31.81±0.06	31.81±0.06
Eridanus Cluster	1	31.99±0.11	31.57±0.13	31.99±0.11
Depth 0.35 mag	1,2	32.01±0.10	31.69±0.11	32.01±0.10
N1395	1	31.97±0.18	31.20±0.20	31.97±0.18
N1400	2	32.19±0.33	32.22±0.27	32.19±0.33
N1407	1	32.30±0.26	31.95±0.19	32.30±0.26
N1426	1	31.89±0.16	31.44±0.32	31.89±0.16
M81 Group	1	27.80±0.08	27.88±0.08	27.87±0.12	28.07±0.15	27.87±0.05
Depth 0.15 mag											
N2366	2	≤27.7:
N2403	2	≤27.5:
N3031	1	27.80±0.08	...	27.88±0.12	28.02±0.28	27.84±0.06
BK5N	1	...	27.88±0.13	27.88±0.13
F8DI	1	...	27.86±0.11	27.86±0.11
U4305	1	≤27.42:
N3184 Group	1	30.79±0.05	30.80±0.06
Depth 0.35 mag											
N3198	1	30.80±0.06	30.80±0.06
N3319	1	30.78±0.10	30.78±0.10
Leo I Group	1,2	30.08±0.06	30.33±0.11	30.01±0.07	...	29.62±0.56	30.30±0.06	30.26±0.07	30.48±0.14	...	30.18±0.03
Depth 0.15 mag											
N3351	1	30.01±0.08	30.01±0.08
N3368	1	30.20±0.10	...	29.91±0.12	30.14±0.23	30.09±0.07
N3377	1	30.10±0.19	30.31±0.12	30.12±0.12	30.19±0.08
N3379	1	...	30.33±0.11	30.01±0.15	...	29.62±0.56	30.18±0.14	30.31±0.12	30.48±0.14	...	30.23±0.06
N3384	1	30.09±0.15	30.38±0.16	30.34±0.11	30.28±0.08
N3627	2	30.06±0.17	30.06±0.17
Coma I Cloud	2	31.41±0.10	...	30.12±0.18	30.74±0.28	...	30.79±0.09	30.96±0.06
Depth 0.52 mag											
N4278	2	30.12±0.18	30.74±0.28	...	31.09±0.21	30.51±0.14
N4414	2	31.41±0.10	31.41±0.10
Coma II Cloud	2	30.57±0.08	...	30.51±0.08	30.44±0.21	...	31.18±0.10	30.68±0.05
Depth 0.52 mag											
N4494	2	30.61±0.09	30.64±0.28	...	31.22±0.13	30.81±0.08

Table 2—Continued

Galaxy	Class ²	$(m - M) \pm \sigma$ Cepheids ³	$(m - M) \pm \sigma$ TRGB ³	$(m - M) \pm \sigma$ PNLF ³	$(m - M) \pm \sigma$ <i>V</i> -GCLF ³	$(m - M) \pm \sigma$ <i>B</i> -GCLF ³	$(m - M) \pm \sigma$ <i>I</i> -SBF ^{3,4}	$(m - M) \pm \sigma$ F814W-SBF ³	$(m - M) \pm \sigma$ <i>K_s</i> -SBF ³	$(m - M) \pm \sigma$ <i>K'</i> -SBF ³	$(m - M) \pm \sigma$ MEAN ⁵
N4565	2	30.20±0.16	30.18±0.32	...	31.26±0.19	30.63±0.12
N4725	2	30.57±0.08	30.67±0.35	30.57±0.08
Virgo Cluster	1	31.04±0.06	30.91±0.10	30.90±0.07	31.29±0.23	...	31.19±0.04	31.09±0.06	30.87±0.09	31.18±0.10	31.07±0.03
M87 subcluster											
Depth 0.21 mag											
IC3388	1	...	30.84±0.10	30.84±0.10
IG Stars	1	...	31.44±0.31	31.44±0.31
N4321	1	31.04±0.09	31.04±0.09
N4374	1	30.99±0.15	31.40±0.14	...	31.42±0.25	...	31.20±0.10
N4382	1	30.83±0.14	31.39±0.17	31.07±0.11
N4406	1	31.03±0.13	31.33±0.12	31.27±0.12	...	31.22±0.15	31.22±0.07
N4458	1	31.17±0.24	30.92±0.13	30.98±0.11
N4473	1	31.04±0.16	31.11±0.13	31.08±0.10
N4478	1	31.34±0.46	...	31.35±0.29	...	31.24±0.17	...	31.35±0.29
N4486	1	30.82±0.12	31.27±0.26	...	31.22±0.16	30.97±0.10
N4489	1	31.31±0.18	...	29.56±0.25	30.75±0.37	31.31±0.18
N4548	1	31.04±0.08	31.48±0.55	31.05±0.08
N4552	1	30.99±0.17	31.02±0.14	30.85±0.13	31.21±0.15	31.01±0.11
N4571	1	≤30.9:
Virgo Cluster	1	31.02±0.04	...	30.79±0.15	31.30±0.27	31.71±0.55	31.07±0.08	31.24±0.13	31.01±0.12	31.18±0.12	31.03±0.03
NGC 4472 subcluster											
Depth 0.21 mag											
N4472	1	30.79±0.15	31.30±0.27	31.71±0.55	31.11±0.13	31.24±0.13	31.25±0.17	31.07±0.15	31.07±0.08
N4496A	1	31.02±0.07	31.02±0.07
N4526	1	31.19±0.22	31.19±0.22
N4535	1	31.10±0.07	31.10±0.07
N4536	1	30.95±0.07	30.95±0.07
N4636	1	30.88±0.16	...	30.79±0.16	31.35±0.18	30.88±0.16
Virgo Cluster	1	31.80±0.09	...	30.82±0.15	...	31.38±0.53	31.22±0.07	30.98±0.08	31.41±0.19	31.31±0.32	31.25±0.04
NGC 4649 subcluster											
Depth 0.21 mag											
N4578	1	31.40±0.15	31.31±0.32	31.40±0.15
N4621	1	31.37±0.22	30.85±0.13	31.41±0.19	...	30.99±0.11
N4639	1	31.80±0.09	31.80±0.09
N4649	1	30.82±0.15	...	31.38±0.53	31.18±0.17	31.23±0.13	31.09±0.08
N4660	1	30.61±0.21	30.76±0.18	30.70±0.14

Table 2—Continued

Galaxy	Class ²	$(m - M) \pm \sigma$ Cepheids ³	$(m - M) \pm \sigma$ TRGB ³	$(m - M) \pm \sigma$ PNLF ³	$(m - M) \pm \sigma$ V-GCLF ³	$(m - M) \pm \sigma$ B-GCLF ³	$(m - M) \pm \sigma$ I-SBF ^{3,4}	$(m - M) \pm \sigma$ F814W-SBF ³	$(m - M) \pm \sigma$ K_s -SBF ³	$(m - M) \pm \sigma$ K' -SBF ³	$(m - M) \pm \sigma$ MEAN ⁵
Cen A Group	1	27.61±0.11	27.93±0.13	27.70±0.11	28.12±0.13	27.82±0.06
Depth 0.67 mag											
N5102	1	27.54±0.22	28.07±0.17	27.89±0.13
N5128	1	...	27.93±0.13	27.76±0.12	28.19±0.19	27.90±0.08
N5253	1	27.61±0.11	...	28.13±0.41	27.61±0.11
M101 Group	1	29.34±0.10	...	29.42±0.13	29.37±0.08
	1+3	29.34±0.10	...	29.47±0.09	30.67±0.13	29.69±0.06
Depth 0.35 mag											
N5195	3	29.52±0.12	29.47±0.28	29.52±0.11
N5457	1	29.34±0.10	...	29.42±0.13	29.37±0.08
N7331 Group	1	30.89±0.10	30.67±0.21	30.85±0.09
	1+2	30.89±0.10	30.67±0.16	30.76±0.15	30.81±0.07
Depth 0.35 mag											
N7331	1	30.89±0.10	30.67±0.21	30.85±0.09
N7457	2	30.66±0.23	30.76±0.15	30.73±0.13
Other Groups											
IC4182	1	28.36±0.08	28.36±0.08
N300	1	26.66±0.10	...	26.93±0.41	26.68±0.10
N2090	1	30.45±0.08	30.45±0.08
N2541	1	30.47±0.08	30.47±0.08
N3115	1	...	30.18±0.30	30.12±0.19	29.90±0.26	...	29.99±0.13	30.05±0.10
N3115DW1	1	30.53±0.84
N3621	1	29.13±0.11	29.13±0.11
N4365	1	31.80±0.39	32.31±0.68	31.61±0.19	...	31.14±0.16	31.86±0.15	31.61±0.19
N4373	1	33.23±0.22	32.76±0.23	33.01±0.16
N4594	1	29.75±0.11	30.01±0.20	29.99±0.17	29.85±0.08
N4603	1
N5170	1	31.50±0.34
N5481	1	31.84±0.56
N5846	1	32.61±0.28	...	32.05±0.22	32.05±0.22

¹References for the original data from which the distances given in this table were derived can be found in Ferrarese et al. (1999).

²Galaxies which are certain, very likely, or just probable members of their assigned group or cluster are designated as class 1, 2, and 3 respectively.

³The errors quoted on the distance moduli are random errors only, with the exception of the ground-based Cepheid distances which include both random and systematic errors. Systematic errors amount to 0.13 mag for TRGB and PNLf distance moduli, and 0.16 mag for GCLF, I -, F814W-, K_s -, and K' -SBF, and all Cepheid distance moduli observed with the *HST*

⁴All I -SBF distances quoted from this table must reference Tonry et al. (1999) and Ajhar et al. (1999) as the source of the SBF measurement, combined with the calibration presented in this paper.

⁵Weighted mean of all of the available Cepheid, PNLf, TRGB, I - and F814W-SBF. GCLF and near infrared SBF measurements are not included for the reasons discussed in §5 and Appendix B.

Table 4. Sample of F814W-SBF Galaxies for Deriving H_0

Cluster	Galaxy ID	RA (J2000)	Dec (J2000)	$(m - M)_0^a$	v_{hel}^b	Δv (YTS)	Δv (IAU)	v (CMB)	v (flow)	H_0^a	H_0^c
NGC 4373	N4373	12:25:19	−39:45:37	32.84±0.23	3395	−263	−206	3625	3118	84±16	80±16
Abell 262	N708	01:52:46	+36:09:06	34.22±0.22	4897	+251	+187	4709	4831	69±8	66±8
Abell 3560 ^d	N5193	13:31:54	−33:14:07	33.60±0.18	3806	−255	−193	4020	3468	66±12	63±11
Abell 3565	IC 4296	13:36:39	−33:57:59	33.77±0.17	3686	−254	−192	3894	3341	59±11	56±10
Abell 3742	N7014	21:07:53	−47:10:40	34.18±0.16	4918	−62	−29	4710	5061	74±7	70±7
Coma	N4881	12:59:58	+28:14:43	35.10±0.55	6965	−29	+9	7191	7441	71±18	68±17
H_0 , all galaxies										70±4	67±4
H_0 , excluding NGC 4881 and NGC 4373										69±4	66±4

^aValues assume no metallicity dependence of the Cepheid PL relation, and $M_I = (-1.70 \pm 0.10) + (4.5 \pm 0.3)[(V - I)_0 - 1.15]$.

^bFrom the CfA redshift survey, Chen et al. (2000).

^cValues assume a metallicity dependence of the Cepheid PL relation as in Kennicutt et al. 1998.

^dThis is in fact a group in the foreground of Abell 3560. The actual Abell 3560 cluster is at $cz \sim 15000 \text{ km s}^{-1}$.